UCRL-PROC-225260

LAWRENCE
LIVERMORE
NATIONAL
LABORATORY

Corrosion Resistances of Iron-Based Amorphous Metals with Yttrium and Tungsten Additions in Hot Calcium Chloride Brine & Natural Seawater: Fe48Mo14CR15Y2C15B6 and Variants

J. Farmer, J. Haslam, S. Day, T. Lian, C. Saw, P. Hailey, J.-S. Choi, N. Yang, C. Blue, W. Peter, J. Payer, J. Perepezko, K. Hildal, D. J. Branagan, M. B. Beardsley, L. Aprigliano

October 12, 2006

Disclaimer

Corrosion Resistances of Iron-Based Amorphous Metals with Yttrium and Tungsten Additions in Hot Calcium Chloride Brine & Natural Seawater: $Fe_{48}Mo_{14}Cr_{15}Y_2C_{15}B_6$ and Variants

J. Farmer[1], J. Haslam[1], S. Day[1], T. Lian[1], C. Saw[1], P. Hailey[1], J-S. Choi[1], N. Yang[2], C. Blue[3], W. Peter[3], J. Payer[4], J. Perepezko[5], K. Hildal[5], D. J. Branagan[6] , M. B. Beardsley[7] and L. Aprigliano[8]

[1]Lawrence Livermore National Laboratory, [2]Sandia National Laboratory, [3]Oak Ridge National Laboratory, [4]Case Western Reserve University, [5]University of Wisconsin Madison, [6]The NanoSteel Company, [7]Caterpillar, and [8]Strategic Analysis Incorporated

ABSTRACT

The passive film stability of several Fe-based amorphous metal formulations have been found to be comparable to that of stainless steels and Ni-based Alloy C-22 (UNS # N06022), based on electrochemical measurements of the passive film breakdown potential and general corrosion rates. Electrochemical studies of the passive film stability of SAM1651 are reported here.

Chromium (Cr), molybdenum (Mo) and tungsten (W) provide corrosion resistance; boron (B) enables glass formation; and rare earths such as yttrium (Y) lower critical cooling rate (CCR). Yttrium-containing SAM1651, also known as SAM7 ($Fe_{48.0}Cr_{15.0}Mo_{14.0}B_{6.0}C_{15.0}Y_{2.0}$), has a critical cooling rate (CCR) of approximately 80 Kelvin per second, while yttrium-free SAM2X5 ($Fe_{49.7}Cr_{17.7}Mn_{1.9}Mo_{7.4}W_{1.6}B_{15.2}C_{3.8}Si_{2.4}$) has a higher critical cooling rate of approximately 600 Kelvin per second. SAM1651's low CCR enables it to be rendered as a completely amorphous material in practical materials processes. While the yttrium enables a low CCR to be achieved, it makes the material relatively difficult to atomize, due to increases in melt viscosity. Consequently, the powders have irregular shape, which makes pneumatic conveyance during thermal spray deposition difficult.

The reference material, nickel-based Alloy C-22, is an outstanding corrosion-resistant engineering material. Even so, crevice corrosion has been observed with C-22 in hot sodium chloride environments without buffer or inhibitor. SAM1651 may also experience crevice corrosion under sufficiently harsh conditions. Both Alloy C-22 and Type 316L stainless lose their resistance to corrosion during thermal spraying, due to the formation of deleterious intermetallic phases which depletes the matrix of key alloy elements, whereas SAM1651 can be applied as coatings with the same corrosion resistance as a fully-dense completely amorphous melt-spun ribbon, provided that its amorphous nature is preserved during thermal spraying. Materials synthesis and characterization is discussed. Data showing the corrosion resistance of SAM1651 in hot concentrated calcium chloride, as well as natural seawater are presented, and compared to a number of reference materials.

INTRODUCTION

This research has two primary long-term goals, all directed towards development of advanced amorphous-metal thermal-spray coatings with corrosion resistance superior to Type 316L stainless steel [UNS # S31603] and nickel-based Alloy C-22 [UNS # N06022]. Computational materials science has been used to help guide the design these new materials.

Novel Fe-Based Amorphous Metal Coatings

Several Fe-based amorphous metal formulations have been found that appear to have corrosion resistance comparable to, or better than that of Ni-based Alloy C-22, based on breakdown potential and corrosion rate [1-3]. These formulations use chromium (Cr), molybdenum (Mo), and tungsten (W) to provide corrosion resistance, boron (B) to enable glass formation, and yttrium to lower the critical cooling rate (CRR). SAM1651 ($Fe_{48.0}Cr_{15.0}Mo_{14.0}B_{6.0}C_{15.0}Y_{2.0}$), which is also known as SAM7, has very low critical cooling rate of approximately 80 Kelvin per second, due to the addition of yttrium.

The SAM1651 formulation has the same nominal elemental composition as the Y-containing Fe-based amorphous metal formulation discussed in the literature [4-6]. These rare-earth containing materials have been selected with particular emphasis on glass forming ability, thermal stability, hardness, and corrosion resistance, all under conditions of interest.

By exploiting the melt spinning process, several alloy compositions of Fe-based amorphous metals have been produced, characterized, and tested. Several of these were compositional modifications of the SAM40 master alloy [7-12], and were prepared by following the general formula: $[(SAM40)_{100-x} + Z_x]$ where Z is the added element, and x is the amount of the addition in atomic percent. Additives investigated included nickel, chromium, molybdenum, tungsten, yttrium, titanium and zirconium. The nickel and molybdenum additions are known to greatly influence the electrochemical properties of conventional stainless steel alloys. The yttrium, titanium, and zirconium additions, while not normally added to steels are known to form very stable oxides and are expected to increase the stability and passivity of the oxide film in a variety of environments.

SAM1651 has a low critical cooling rate (CCR), due to the addition of yttrium (Y), which enables it to be rendered as a completely amorphous thermal spray coating. The yttrium addition increases the viscosity of the alloy, thereby slowing the nucleation and growth kinetics of crystalline phases. Unfortunately, such increases in viscosity also make this material relatively difficult to gas atomize, with the powders having irregular shapes. Such non-spherical particle morphology causes pneumatic conveyance of the SAM1651 powder during thermal spray operations to be difficult. The production of nearly spherical gas-atomized SAM1651 powder with acceptable flow characteristics has required extensive particle sorting, exotic and expensive milling to eliminate irregularities, and significant process optimization.

Protective coatings of nickel-based Alloy C-22 and Type 316L stainless can be applied with thermal spray technology [13]. However, their corrosion resistance is lost at the high temperatures required for deposition. Based upon extensive studies of these austenitic alloys in

wrought form, it is believed that this loss in corrosion resistance may be due to the precipitation of undesirable phases (P, σ, and μ). These precipitated phases deplete the matrix of those alloying elements responsible for passivity. In contrast, SAM1651 (SAM7) coatings can be applied with thermal spray processes without any significant loss of corrosion resistance.

It is important to point out that the outstanding corrosion possible with amorphous metals has been recognized for many years [14-16]. A number of other iron-based amorphous metals have been published, including several with very good corrosion resistance. Examples include: thermally sprayed coatings of Fe-10Cr-10-Mo-(C,B) which were explored as early as 1996 by Kishitake et al. [17]; bulk Fe-Cr-Mo-C-B [18]; and Fe-Cr-Mo-C-B-P [19]. These authors have corroborated the outstanding corrosion resistance of the amorphous Fe-Cr-Mo-C-B-P alloys [18]. Nickel-based amorphous metals have also been developed which exhibit exceptional corrosion performance in acidic environments [20].

Other Attributes of Fe-Based Amorphous Metal Coatings

Such materials are extremely hard, and provide enhanced resistance to abrasion and gouges (stress risers) from backfill operations, and possibly even tunnel boring. The hardness of Type 316L Stainless Steel is approximately 150 VHN, that of Alloy C-22 is approximately 250 VHN, and that of HVOF SAM1651 (SAM7) ranges from 1100-1300 VHN [7]. SAM1651 coatings can be applied with thermal spray processes without any significant loss of corrosion resistance.

SAM1651 has significant boron (B) content, which should enable them to absorb neutrons and therefore be used for criticality control in baskets. The possibility of incorporating other neutron absorbers such as gadolinium (Gd) also exists. Alloy C-22 and 316L have no neutron absorber, and cannot be used for such functions. Borated stainless steel and Gd-doped Ni-Cr-Mo alloys are being developed but may face limitations related to their availability, cost, corrosion and leach resistance, and mechanical properties. Tests with J-13 well waters have shown that boron can preferentially leach boron, the neutron absorber, from borated stainless steels. Well J-13 water has a typical water chemistry for saturated zone and perched waters at Yucca Mountain and a mean composition that was reported by Harrar et al. [21]. During evaporation of J-13 water, Na^+, K^+, Cl^-, and NO_3^- are concentrated, and HCO_3^-, Ca^{2+} and Mg^{2+} can be removed from solution by the precipitation of calcium and magnesium carbonate.

Importance of Chromium, Molybdenum and Tungsten

The importance of chromium, molybdenum and tungsten additions to amorphous metals as a means of enhancing corrosion resistance is discussed in this section. The decision to achieve enhanced corrosion resistance in these Fe-based amorphous metals was initially based upon two considerations. First, substantial enhancements in corrosion resistance had been observed in stainless steels and nickel based alloys by adding molybdenum, as well as other alloying elements. Secondly, this enhancement in localized corrosion resistance can be quantified in the pitting resistance equivalence number, and could be used as a guide to determine the level of molybdenum addition necessary to achieve localized corrosion resistance comparable to nickel-based Alloy C-22, one of the benchmark materials. Branagan et al. used estimates of PREN to determine the maximum concentration of various alloying elements to be added to an amorphous-metal master alloy, so that the relationship between composition and corrosion resistance of families of Fe-based amorphous metals could be systematically explored by this

group [1-3]. Based upon these calculations, it was believed that SAM7 (SAM1651) and SAM8 compositions possessed enough chromium, molybdenum, tungsten, yttrium and other constituents to demonstrate passive film stability comparable to nickel-based Alloy C-22. This hypothesis has been tested in this investigation, and found to have merit.

The importance of molybdenum in nickel-based alloys has been recognized for many years. Alloy C-22 (UNS N06022) is now being considered for construction of the outer barrier of the WP. This alloy consists of 20.0-22.5% Cr, 12.5-14.5% Mo, 2.0-6.0% Fe, 2.5-3.5% W, 2.5% (max.) C, and balance Ni. Alloy C-22 is less susceptible to localized corrosion in environments that contain Cl⁻ than Alloys 825 and 625, materials of choice in earlier designs. The unusual localized corrosion resistance of Alloy C-22 is apparently due to the additions of Mo and W, both of which are believed to stabilize the passive film at very low pH [22]. The oxides of these elements are very insoluble at low pH. Consequently, Alloy 22 exhibits relatively high thresholds for localized attack. High repassivation potentials have been observed by some [23], while others have found very low corrosion rates in simulated crevice solutions containing 10 wt. % $FeCl_3$ [24].

EXPERIMENTAL PROCEDURES

Melt Spinning Process

The development of an appropriate powder composition for the production of a corrosion-resistant thermal-spray coating requires that the alloy first be tested in a form with no porosity, and with little or no crystalline phases present. Testing of such materials enables determination of the best possible corrosion performance for a given composition. Melt spinning and arc-melting with drop casting have been used as methods to synthesize completely amorphous, Fe-based, corrosion-resistant alloys with near theoretical density, thereby enabling the effects of coating morphology on corrosion resistance to be separated from the effects of elemental composition.

Cooling rates approaching one billion Kelvin per second (10^9 K/s) may be achieved with physical vapor deposition (PVD), and can be used to produce amorphous metal thin films. However, other processes are required to produce free-standing materials and coatings of practical thickness for corrosion and wear resistance. The thickness of PVD films is typically one to five microns (1-5 μm). Maximum cooling rates of one million Kelvin per second (10^6 K/s) have been achieved with melt spinning, and is therefore ideal for producing amorphous metals over a very broad range of compositions. The melt-spun ribbon (MSR) samples produced with this equipment are several meters long, several millimeters wide and approximately 150 microns thick [7]. In contrast, the cooling rate in a typical thermal spray process such as HVOF are on the order of ten thousand Kelvin per second (10^4 K/s). The compositional range of materials that can be rendered as amorphous metals with thermal spray is therefore more restricted.

The melt spinning involves the ejection of a liquid melt onto a rapidly moving copper wheel with a pressure-controlled gas. The liquid melt solidifies onto the wheel, with subsequent separation from the wheel by thermal contraction and centrifugal force, and collection in a chamber. By changing the tangential velocity of the wheel, as well as other processing parameters, the cooling rate can be controlled over a very broad range. The specific processing parameters for the melt-

spinning process can be selected to establish cooling rates that are representative of a given thermal spray process. If a specific cooling rate produces an amorphous, glassy metal during melt spinning, it should also produce a glassy structure during thermal spray. It is therefore possible to use melt spinning to simulate the type of microstructure that can be achievable with thermal spraying, such as the high-velocity oxy-fuel process. Furthermore, an entire series of developmental materials, with different compositions, heat capacities, and thermal conductivity, can be made with the same cooling rates, so that the ease of processing each can be compared.

By exploiting the melt spinning process, several alloy compositions of Fe-based amorphous metals have been produced, characterized, and tested [1-3]. Several of these were compositional modifications of the SAM40 master alloy [7-12], and were prepared by following the general formula: $[(SAM40)_{100-x} + Z_x]$ where Z is the added element, and x is the amount of the addition in atomic percent [7]. Additives investigated included nickel, chromium, molybdenum, tungsten, yttrium, titanium and zirconium. The nickel and molybdenum additions are known to greatly influence the electrochemical properties of conventional stainless steel alloys. The yttrium, titanium, and zirconium additions, while not normally added to steels are known to form very stable oxides and are expected to increase the stability and passivity of the oxide film in a variety of environments. The SAM1651 formulation has the same nominal elemental composition as the Y-containing Fe-based amorphous metal formulation discussed in the literature [4-6]. These rare-earth containing materials have been selected with particular emphasis on glass forming ability, thermal stability, hardness, and corrosion resistance, all under conditions of interest.

The melt-spinning process was used to perform a systematic study of various elemental compositions, each based on the Fe-based SAM40 master alloy, with 1, 3, 5, and 7 atomic percent additions of specific elements believed to be beneficial to glass formation or corrosion resistance. The alloy compositions explored during this study are summarized in Tables 1 and 2. Elemental additions investigated included nickel, molybdenum, yttrium, titanium, zirconium, and chromium. The densities of the amorphous metals prepared with melt spinning were determined, and all were less dense than nickel-based N06022 (Alloy C-22), and therefore offer a weight advantage over such classical corrosion-resistant alloys. The first re-crystallization peak for each of melt-spun ribbons was determined with differential thermal analysis (DTA), and was similar to that of a master alloy (SAM40). The formula with the yttrium additions showed re-crystallization peaks at higher temperatures than achieved with other formulae, corroborating the fact that yttrium additions do indeed promote thermal stability and glass formability. Some formulae exhibited a second re-crystallization process at a higher temperature than the first, with titanium and zirconium based formulations showing these processes at the highest temperatures. All of the "as-cast" amorphous metal formulae produced by the HPCRM Team exhibited hardness far superior to many of the conventional materials of interest, such as Type 316L stainless steel, and nickel-based N06022 (Alloy C-22). Thus, coatings of these materials would also be expected to be less prone to erosion, wear and gouging than conventional engineering alloys. Partially de-vitrified samples of the HPCRM materials exhibited dramatic increases in hardness. Thus, carefully controlled heat treatment of these materials can be used to achieve dramatic improvements in resistance to erosion, wear and penetration.

Thermal Spray Process

Several thermal spray processes have been developed by industry and include: flame spray, wire-arc; plasma spray; water-stabilized plasma spray; high-velocity oxy-fuel; and the detonation gun. Any of these can be used for the deposition of Fe-based amorphous metals, with varying degrees of residual porosity and crystalline structure. The coatings discussed here were made with the high-velocity oxy-fuel (HVOF) process, which involves a combustion flame, and is characterized by gas and particle velocities that are three to four times the speed of sound (mach 3 to 4). This process is ideal for depositing metal and cermet coatings, which have typical bond strengths of 5,000 to 10,000 pounds per square inch (5-10 ksi), porosities of less than one percent (< 1%) and extreme hardness.

Optimization of the thermal spray process through careful selection of powder size and process temperature, has now yielded coatings of SAM40 (non-optimized elemental coating) that are virtually pore-free, and for all practical purposes, fully dense. These new coating architectures have also been shown, through detailed examination with X-ray diffraction (XRD) and scanning electron microscopy (SEM), to be amorphous. An optimized thermal spray process is now being used to render SAM1651 amorphous metal formulations as high-performance corrosion-resistant coatings, with nearly full density, no significant porosity, and good bond strength.

Energy Dispersive Analysis with X-Rays – Composition

Electron microanalysis of melt-spun ribbons was performed on a series of Fe-based formulations and on Alloy C-22 and Type 316L stainless reference materials. Scanning electron microscopy (SEM) was used to image superficial microstructure using both secondary and backscattered electron detectors. Semi-quantitative elemental composition of the melt-spun ribbons was determined with energy-dispersive X-ray spectroscopy (EDS, EDAX).

Segments of each ribbon were imaged using a Quanta Series 200 environmental scanning electron microscope (ESEM). Images were obtained from both sides of the ribbon, using both secondary electron and back-scattered electron detectors. The side of each ribbon that had been in contact with the melt-spinning copper wheel was distinguishable as being noticeably rougher than the non-contact side.

Semi-quantitative elemental composition was determined with EDS. Compositional analysis was performed on the smoother side of each ribbon, as the rougher sides were found in some cases to be contaminated with small amounts of copper, presumably from contact with the copper wheel during the melt spinning process. Quantification of the light elements, such as boron (B) and carbon (C), was found to be unreliable for these complex sample formulations. The given (formulation) values for these elements were therefore assumed and used in calculating the compositional values for the remaining heavier elements. Microanalysis of each sample was performed at three randomly-selected locations at 10,000X magnification, with the average being reported here.

X-Ray Diffraction – Crystal Structure

The basic theory of X-ray diffraction of amorphous materials is well developed and has been published in the literature [25,26]. A brief summary is presented here to place experimental data for the Fe-based amorphous metals in proper perspective. For crystalline diffraction, specific x-

ray peaks can be observed from a diffraction pattern acquired from x-ray diffractometer for crystalline materials. These peaks are the results of constructive interference of the probing X-ray wave. If the sample is single crystal, these peaks have specific arrangements and orientations. The positions and intensities of these peaks are related to the atomic arrangements in the unit cell of the crystals. Unit cells have 3 axes with 3 angles (called lattice parameters), and they can be grouped into triclinic, monoclinic, orthorhombic, tetragonal, hexagonal, rhombohedral or cubic structures. In general, specific compounds have specific lattice parameters and the compounds can be identified by these parameters. The lattice parameters consist of three axes and three angles.

In an amorphous material, the atoms are not arranged in a periodic fashion such that crystals can be formed. There are broad diffraction peaks, which belong to the amorphous structure. The amorphous state does have structure as defined by the radial distribution function and the partial radial distribution, if it is a multiple elements system. For the present effort, such an analysis is not necessary at the moment. The degree of crystalline structure is correlated to the intensity of each scattering component.

The X-ray diffraction experiment is carried out using the Philip vertical goniometer in the para-focusing or also known as the Bragg-Bretano method. The X-ray optics are self-focusing, and the distance between the X-ray focal point to the sample position is equal to the distance between the sample position and the receiving slit for the reflection mode. Thus, the intensity and resolution are optimized. Parallel vertical slits are also added to improve the scattering signal.

Scintillation detectors are used in most modern X-ray diffractometers. However, the energy resolution is not sufficient to discriminate fluorescence X-rays of certain elements with energy close to the probing X-ray energy. Hence, very often, an analyzing crystal is used after the receiving slit. The choice of the crystal is based on the crystal mosaic, for energy selectivity and the efficiency. The most widely use energy discriminator is usually graphite for efficiency without significantly scarifying X-ray intensity. This is particularly important for the HPCRM because of the iron content in the samples. Iron fluorescence has energy which is close to that of the copper K_α probing X-ray. Sometime X-ray filters are used.

In the present setup, CuK_α is used with a graphite analyzing crystal. Step scan is performed from 20 to 90° (2θ) with step size of 0.02° at 4-10 seconds per point, depending on the amount of sample. The samples are loaded onto low quartz holders. This is because the expected intensity is very low and hence background scattering needs to be minimized.

Thermal Properties

The thermal properties of these Fe-based amorphous metals have been determined. Thermal analysis of these Fe-based amorphous metals, with differential scanning calorimetry (DSC) or differential thermal analysis (DTA), allows determination of important thermal properties such as the glass transition temperature T_g, crystallization temperature T_x and melting interval T_m-T_L. Results from the thermal analysis of amorphous samples provides initial assessment of the glass forming ability of these samples through conventional metrics such as T_{rg} (T_g/T_L), T_x (=T_x-T_g) and γ (=$T_x/(T_g+T_L)$) that can be used to rank alloys based on the expected suitability for thermal spray processing. However, note that the metrics provided by thermal analysis are only initial

assessments, and more detailed studies are required to determine the glass formability of a particular alloy.

Perepezko and his colleagues have also used wedge casting allows accurate determination the cooling rate required to avoid crystallization of the melt upon continuous cooling. A continuous range of cooling rates can be experienced simultaneously by an amorphous metal formulation by casting into a wedge-shaped mold for solidification. Then, examination of the wedge-shaped ingot's microstructure as a function of position reveals the lowest possible cooling rate (correlated with position) that can be used to maintain the material in a glassy state. The cooling rates in the wedge can be predicted with finite element modeling, and can be determined experimental with optical pyrometers (or other comparable methods).

In order to use amorphous coatings in application such as nuclear waste storage, it is crucial to determine the long-term stability of the amorphous phase, as precipitation of crystalline phases such as bcc-Fe will severely reduce the overall corrosion resistance of the coating. A convenient way to visualize thermal stability is the calculation of Time-Temperature-Transformation (TTT) curves that consists of the loci of time-temperature for the onset of nucleation of crystalline phases occurs. A kinetic model as been developed that combines information from wedge casting experiments and isothermal annealing experiments and incorporates these into a heterogeneous nucleation model. Based on this model, TTT-diagrams have been assessed for alloys SAM35 and SAM40, whereas work is in progress (preliminary results are available) for determining the TTT-curves for SAM7 (SAM1651) and other alloys of interest.

Mechanical Properties

Hardness is an important parameter that has impact on wear resistance, as well as the resistance to erosion-corrosion. Vickers micro-hardness (HV) is the standard approach used to assess the hardness of thermal spray coatings. In the specific case of thermal spray coatings, a 300-gram load is frequently used, since it is believed that this load and the affected area are large enough to produce a measurement that is averaged over any macro-porosity that may be present. These authors also like to report micro-hardness measurements with a 100-gram load, since it is believed that this load and the affected area are smaller, and therefore capable of sampling bulk material properties. Typical ranges of the measured micro-hardness for these HVOF coatings are summarized in Table 4.

Cyclic Polarization – Passive Film Stability

Spontaneous breakdown of the passive film and localized corrosion require that the open-circuit corrosion potential exceed the critical potential. The resistance to localized corrosion is quantified through measurement of the open-circuit corrosion potential (E_{corr}), the breakdown potential ($E_{critical}$) and the repassivation potential (E_{rp}). The greater the difference between the open-circuit corrosion potential and the repassivation potential (ΔE), the more resistant a material is to modes of localized corrosion such a pitting and crevice corrosion. In integrated corrosion models, general corrosion is invoked when E_{corr} is less than $E_{critical}$ ($E_{corr} < E_{critical}$), and localized corrosion is invoked when E_{corr} exceeds $E_{critical}$ [13]. The data provided in this publication are sufficient to establish when general and localized corrosion occur, and the rates of general corrosion are when general corrosion is invoked. Note that these data only apply for the environments explored during testing.

Cyclic polarization (CP) is used as a means of measuring the critical potential ($E_{critical}$) of corrosion resistant materials, relative to their open-circuit corrosion potential (E_{corr}). In the published scientific literature, different bases exist for determining the critical potential from electrochemical measurements. The critical potential is frequently defined as the point where the passive current density increases during the forward (anodic) scan to a level between 1 to 10 μA/cm^2 (10^{-6} to 10^{-5} A/cm^2). Alternative definitions of the repassivation potential are used. One definition is the point during the reverse (cathodic) scan where the current density drops to a level indicative of passivity, which is *assumed* to be between 0.1 to 1 μA/cm^2 (10^{-6} to 10^{-7} A/cm^2). An alternative definition is the point where the forward and reverse scans intersect, a point where the current density being measured during the reverse scan drops to a level *known* to be indicative of passivity. These authors prefer the latter definition.

Definitions of the threshold and repassivation potentials vary from investigator to investigator. Gruss et al. define the repassivation potential as the point where the current density drops to 10^{-6} to 10^{-7} A cm^{-2} [23]. Scully et al. define the threshold potential for crevice corrosion of Alloy 22 as the point during the scan of electrochemical potential in the forward direction where the current density increases to a level of 10^{-6} to 10^{-5} A cm^{-2}. Scully et al. generated CP data with very tight crevices and concentrated electrolytes consisting of 5M LiCl, 0.024 to 0.24M NaNO$_3$, 0.026 to 0.26M Na$_2$SO$_4$ and HCl [27]. Testing was conducted at two temperature levels, 80 and 95°C. The crevices were formed with a multiple crevice former, PTFE tape, and an applied torque of 70 inch pounds. Under these circumstances, some electrochemical activity indicative of crevice corrosion was observed at potentials ranging from 71 to 397 mV versus Ag/AgCl, depending upon the composition of the electrolyte. Using a current density criterion for repassivation of 10^{-5} A cm^{-2}, repassivation potentials were determined to be slightly above, but relatively close to the open-circuit corrosion potential.

Cyclic polarization measurements have been based on a procedure similar to ASTM (American Society for Testing and Materials) G 5 standard with slight modification [28-31]. The ASTM G 5 standard calls for a 1 N H$_2$SO$_4$ electrolyte, whereas synthetic bicarbonate, sulfate-chloride, chloride-nitrate, and chloride-nitrate solutions, with sodium, potassium and calcium cations, as well as natural seawater have been used for this investigation. The chloride anion promotes passive film breakdown, while the nitrate serves as an inhibitor. Furthermore, the ASTM G 5 standard calls for the use of de-aerated solutions, whereas aerated and de-aerated solutions were used here. After a 24-hour hold period, during which the open circuit corrosion potential is determined, the potential is scanned in the positive (anodic) direction from a level slightly more negative than the corrosion potential (cathodic limit), to a reversal potential (E_{rev}) near that required for oxygen evolution (anodic level). During the positive scan, anodic oxidation peaks may be observed (centered at E_{peak}) that have been correlated with the oxidation of molybdenum at the alloy surface (passive film), as well as current excursions that are usually associated with breakdown of the passive film. During the negative (cathodic) scan, a hysteresis loop will be observed in cases where passivity has been lost. As the scan continues, the current density may eventually decrease to a level equivalent to that experienced during the positive scan, and indicative of reformation of the passive film. The potential at which this occurs is known as the repassivation potential (E_{rp}).

Temperature-controlled borosilicate glass (Pyrex) electrochemical cells were used for cyclic polarization and other similar electrochemical measurements. This cell has three electrodes, a working electrode (test specimen), the reference electrode, and the counter electrode. A standard silver silver-chloride electrode, filled with near-saturation potassium chloride solution, is used as the reference, and communicates with the test solution via a Luggin probe placed in close proximity to the working electrode, thereby minimizing Ohmic losses. Numerical corrections for the reference electrode junction potential have been estimated, and have been found to be insignificant. The electrochemical cell is equipped with a water-cooled junction to maintain reference electrode at ambient temperature, thereby maintaining integrity of the potential measurement, and a water-cooled condenser to prevent the loss of volatile species from the electrolyte. All powder used to produce these coatings was produced by The NanoSteel Company (TNC), and the HVOF coatings used to generate the data in this publication were produced by Plasma Technology Incorporated (PTI). Synthetic brine solutions (5M $CaCl_2$ and others) were prepared at Lawrence Livermore National Laboratory with reagent-grade chemicals and de-ionized water. The natural seawater used in these tests was obtained directly from Half Moon Bay along the northern coast of California, and was transported to the laboratory in a clean polyethylene container. This Half Moon Bay seawater is referred to as natural seawater in this publication.

Cyclic Polarization – Alloy Screening

Cyclic polarization of melt spun ribbons was further used to compare the relative corrosion resistance of a large number candidate alloy compositions in near-boiling natural seawater at 90°C. As previously discussed, the alloy compositions explored during this study are summarized in Tables 1 and 2. The difference between the open circuit corrosion potential (E_{corr}) and the repassivation potential (E_{rp}) was used as a basis of comprison for the relative corrosion performance of candidate alloys. Several of the candidate alloy compositions had a larger metric value (E_{rp}- E_{corr}) than the reference material, which has been established as nickel-based Alloy C-22, due to its own outstanding corrosion performance. During this early phase of the study, it was concluded that several types of iron-based amorphous metals exist which all have passive film stabilities in seawater at 30°C and 90°C that are comparable to that of the reference material [1-3].

Potentiostatic Step – Threshold for Passive Film Breakdown

Potentiostatic step tests have been used to determine the potential at which the passive film breaks down on the reference material, Alloy C-22, and on the two amorphous metals of primary interest, SAM1651. During prolonged periods of at a constant applied potential (potentiostatic polarization), which are typically 24 hours in duration, the current is monitored as a function of time. In cases where passivity is lost, the current increases, and the test sample is aggressively attacked. In cases where passivity is maintained, the current decays to a relatively constant asymptotic level, consistent with the known passive current density. In these tests, periods of polarization are preceded by one hour at the open circuit corrosion potential.

All were tested in natural seawater heated to 90°C. To eliminate the need for surface roughness corrections in the conversion of measured current and electrode area to current density, the SAM1651 coatings were polished to a 600-grit finish prior to testing. The constant potential denoted in the figures was applied after 1 hour at the open circuit corrosion potential (OCP).

Effect of Devitrification on Corrosion Resistance

To assess the sensitivity of these iron-based amorphous metals to devitrification, which can occur at elevated temperature, melt-spun ribbons of Fe-based amorphous metals were intentionally devitrified by heat treating them at various temperatures for one hour. After heat treatment, the samples were evaluated in low temperature seawater (30°C), to determine the impact of the heat treatment on passive film stability and corrosion resistance. The temperatures used for the heat treatment were: 150, 300, 800 and 1000°C. Untreated (as received) ribbons were also tested, and provide insight into the baseline performance.

Determining Corrosion Rate with Linear Polarization

The linear polarization method has been used as a method for determining the corrosion rates of the various amorphous metal coatings, including SAM7 (SAM1651). This method is based upon experimental determination of electrokinetic parameters in the classic Tafel equation with a potentiostat. The classic Butler-Volmer expression collapses into the well-known anodic Tafel equation at high anodic potential, where the contribution of the electrochemical reduction (cathodic) reaction to the overall current at the electrode surface becomes insignificant (defined as < 1%). At high cathodic potential, where the contribution of the electrochemical oxidation (anodic metal dissolution) reaction to the net electrode current is insignificant, the Butler-Volmer expression becomes the cathodic Tafel equation. The procedure used for linear polarization testing consists of the following steps: (1) hold the sample for ten (10) seconds at the open circuit potential (OCP); (2) beginning at a potential 20 mV below the OCP (OCP-20 mV), increase the potential linearly at a constant rate of 0.1667 mV per second, to a potential 20 mV above the OCP (OCP+20 mV); (3) record the current being passed from the counter electrode to the working electrode by the potentiostat, as a function of potential relative to the standard/silver silver-chloride (Ag/AgCl) reference electrode; and (4) determine the parameters in the cathodic Tafel line by performing linear regression on the voltage-current data from 10 mV below the OCP (OCP – 10 mV) to 10 mV above the OCP (OCP + 10 mV). The slope of this line is the polarization resistance, Rp (ohms), which is defined as [33]:

$$R_P = \left(\frac{\partial E}{\partial I} \right)_{E_{corr}}$$

A parameter (B) is defined in terms of the slopes of the anodic and cathodic branches of the Tafel line:

$$B = \frac{\beta_a \beta_c}{2.303(\beta_a + \beta_c)}$$

Values of B are published for a variety of iron-based alloys, and vary slightly from one alloy-environment combination to another [33]. Values for carbon steel, as well as Type 304, 304L and 430 stainless steels, in a variety of electrolytes which include seawater, sodium chloride, and sulfuric acid, range from 19 to 25 mV. A value for nickel-based Alloy 600 in lithiated water at 288°C is given as approximately 24 mV. While no values have yet been developed for the Fe-based amorphous metals that are the subject of this investigation, it is believed that a

conservative representative value of approximately 25 mV is appropriate for the conversion of polarization resistance to corrosion current. Given the value for Alloy 600, a value of 25 mV is also believed to be acceptable for converting the polarization resistance for nickel-based Alloy C-22 to corrosion current. The corrosion current, I_{corr} (A) is then defined as:

$$I_{corr} = \frac{B}{R_p}$$

where the parameter B is conservatively assumed to be approximately 25 mV. The corrosion current density, i_{corr} (A cm^{-2}), is defined as the corrosion current, normalized by electrode area, and is:

$$i_{corr} = \frac{I_{corr}}{A}$$

A is the surface area of the sample in square centimeters (cm^2). The corrosion (or penetration) rate of an alloy can be calculated from the corrosion current density with the following formula derived from Jones [34]:

$$\frac{dp}{dt} = \frac{i_{corr}}{\rho_{alloy} \, n_{alloy} \, F}$$

where p is the penetration depth, t is time, i_{corr} is the corrosion current density, ρ_{alloy} is the density of the alloy (g cm^{-3}) , n_{alloy} is the number of gram equivalents per gram of alloy, and F is Faraday's constant. The value of n_{alloy} can be calculated with the following formula:

$$n_{alloy} = \sum_j \left(\frac{f_j n_j}{a_j} \right)$$

where f_j is the mass fraction of the jth alloying element in the material, n_j is the number of electrons involved in the anodic dissolution process, which is assumed to be congruent, and a_j is the atomic weight of the jth alloying element. Congruent dissolution means that the dissolution rate of a given alloy element is proportional to its concentration in the bulk alloy. These equations have been used to calculate factors for the conversion of corrosion current density to the penetration rate (corrosion rate). These conversion factors are summarized in Table 5.

An equivalent expression that frequently appears in the literature for calculation of the penetration rate, referred to in this case as the corrosion rate, CR (mm y^{-1}), is also given:

$$CR = \left(K \times i_{corr} \times EW \right) / \rho_{alloy}$$

The parameter K is a conversion factor has a value of (3.27×10^{-3} mm·g·μA^{-1}·cm^{-1}·yr^{-1}), the corrosion current density i_{corr} is given in the units (μA cm^{-2}), and EW is the equivalent weight of the alloy.

Effects of Junction Potential on Electrochemical Measurements

It is important to understand the magnitude of the error in the potential measurements due to the junction potential. A correction has been performed based upon the Henderson Equation, as presented by Bard and Faulkner [35]. The calculated junction for several test solutions have been estimated with ionic properties used in the calculation were also taken from Bard and Faulkner. These corrections are not very large, with the largest being less than approximately 10 mV. This value corresponds to the junction potential for SSW at 90°C. It is concluded that insignificant error results from neglecting to correct for the junction potential.

Validation with Salt Fog Testing

The corrosion resistance of the amorphous metal coatings was verified during salt fog testing. As previously discussed, the salt fog test was used to compare various wrought ant thermal-spray alloys, melt-spun ribbons, arc-melted drop-cast ingots, and thermal-spray coatings for their susceptibility to corrosion by salt sprays, like those that might be encountered aboard naval ships. This test is also known as the salt spray test. The most recent tests have focused on reference materials and the SAM7 (SAM1651) amorphous metal formulation, in the form of arc-melted drop-cast ingots, melt-spun ribbons, and high-velocity oxy-fuel coatings with no significant porosity and near theoretical density. In contrast, the first tests focused on early thermal-spray coatings, which had residual porosity and crystalline structure, and lower resistance to corrosion.

Both salt fog tests were conducted according to the standard General Motors (GM) salt fog test, identified as GM9540P, which is similar to the standard American Society for Testing and Materials (ASTM) salt fog test, which is identified as ASTM B117 and entitled "Standard Test Method of Salt Spray (Fog) Testing." The test protocol for GM9540P is summarized in Table 6. Samples of iron-based amorphous-metal thermal spray coatings and several reference samples were evaluated with the GM9540P test protocol. The four reference samples included Type 316L stainless steel, nickel-based Alloy C-22 (N06022), Ti Grade 7, and the 50:50 nickel-chromium binary.

EXPERIMENTAL RESULTS

Composition of Amorphous Metals

Several Fe-based amorphous metals were systematically explored during this investigation, with the compositions of the yttrium-containing variants summarized in Table 1. Additions of molybdenum (Mo), chromium (Cr) and tungsten (W) were added to enhance passivity; boron (B) was added to enable glass formation; and yttrium (Y) was added to lower critical cooling rate (CRR). The compositions of melt-spun ribbon samples were verified with energy dispersive X-ray spectroscopy (EDAX) and are summarized in Table 2.

Figure 1 shows X-ray diffraction (XRD) data for melt-spun ribbon (MSR) samples of Type 316L stainless steel and nickel-based Alloy C-22. The strong peaks are indicative of the crystalline nature of these materials. Figure 2 shows X-ray diffraction data for melt-spun ribbon (MSR)

samples of iron-based amorphous metals identified as: (a) SAM40; (b) SAM7, which is also known as SAM1651; and (c) SAM8 are completely amorphous, as expected.

Thermal Properties

SAM3X1 has a glass transition temperature of ~560°C, a crystallization temperature of ~614°C, a melting point of ~1108°C, and a reduced glass transition temperature of ~0.52. SAM3X5, which has significantly more yttrium than SAM3X1, has a glass transition temperature of ~590°C, a crystallization temperature of ~677°C, a melting point of ~1143°C, and a reduced glass transition temperature of 0.52. In contrast, the yttrium-containing SAM1651 (SAM7) formulation has a glass transition temperature of ~584°C, a crystallization temperature of ~653°C, a melting point of ~1121°C, and a reduced glass transition temperature of ~0.55. The critical cooling rate of SAM1651 has been determined to be ≤ 80 K per second, which is significantly less than other corrosion-resistant iron-based amorphous metals such as SAM2X5. Clearly, the yttrium additions in SAM1651 enhance glass-forming ability of these materials. Table 3 summarizes these thermal properties for SAM3X1 through SAM3X7, SAM7 (SAM1651), and SAM8.

Cyclic Polarization Polarization

Cyclic polarization data for three drop-cast ingots of SAM1651 (SAM7) Fe-based amorphous metal with yttrium in three different environments is shown in Figure 3: seawater at 90°C; 3.5 molal NaCl at 90°C; and 5M CaCl$_2$ at 105°C. All three cyclic polarization curves show outstanding passivity.

Cyclic polarization data for a wrought prism of nickel-based Alloy C-22, a drop-cast ingot of iron-based SAM7 (SAM1651) amorphous metal, and a melt-spun ribbon of SAM8 (SAM1651 or SAM7 + 3 atomic percent tungsten), all obtained with 5M CaCl$_2$ at 105°C is shown in Figure 4. Both the SAM7 (SAM1651) and SAM8 showed passive film stability comparable to (or better than) Alloy C-22. The addition of 3 atomic-percent tungsten to the SAM7 (SAM1651) enhanced the passive film stability, and also yielded more ductile and damage-tolerant amorphous metal ribbons.

Potentiostatic Data – Natural Seawater at 90°C

Potential-step testing in deaerated seawater heated to 90°C has been performed with SAM1651 (SAM7) and Alloy C-22 thermal spray coatings, as well as wrought Alloy C-22, as shown in Figure 5. The natural seawater used in these tests was obtained directly from Half Moon Bay along the northern coast of California. Tests were also performed on the reference material, Alloy C-22, in both wrought and thermally sprayed condition. To eliminate the need for surface roughness corrections in the conversion of measured current and electrode area to current density, the SAM1651 (SAM7) coating was polished to a 600-grit finish prior to testing. The Alloy C-22 thermal spray coating was tested in the as-sprayed condition, so a roughness factor must be applied to convert the apparent current density into actual current density. The curves represent the asymptotic current density reached after 24 hours at the corresponding potential. In this series of experiments, the passive film on wrought Alloy C-22 also commences breakdown at a potential of approximately 600 mV above the open circuit corrosion potential. Passive film breakdown on the HVOF coating of SM1651 occurred at an applied potential between 500 and

600 mV, where breakdown occurred at approximately 400 mV for the Alloy C-22 HVOF coating. In near-boiling seawater, the passive film stability of SAM1651 (SAM7) is comparable to that of Alloy C-22.

Current transients at various levels of constant applied potential ranging from (100 to 1000 mV vs. OCP) in deaerated seawater at 90°C, for wrought nickel-based Alloy C-22 (serial number CC-22 4007), and are shown in Figure 6. These measured transients are indicative of good passive film stability at the lower applied potentials. This sample was polished to a 600-grit finish, and has a surface area of approximately one square centimeter. At 700 to 800 mV vs. OCP, the current, which is close in value to the current density, rose to a point where the material was losing passivity (greater than 10 μA/cm^2).

Current transients were measured at various levels of constant applied potential (100 to 800 mV vs. OCP) in seawater at 90°C, for a 600-grit polished SAM1651 (SAM7) HVOF coating on Type 316L stainless steel (serial number E316L409), and are shown in Figure 7. These measured transients are indicative of good passive-film stability, which is comparable to that of wrought Alloy C-22. To eliminate the need for surface roughness corrections in the conversion of measured current and electrode area to current density, the SAM1651 (SAM7) coating was polished to a 600-grit finish prior to testing. Passive film breakdown on the HVOF coating of SM1651 occurred at an applied potential between 500 and 600 mV vs. OCP, with a clear loss of passivity at 700 mV. The coating represented by this figure is one of the first known thermal spray coatings with the SAM1651 (SAM7) composition.

Current transients were measured at various levels of constant applied potential (100 to 500 mV vs. OCP) in seawater at 90°C, for an as-sprayed (unpolished) Alloy C-22 HVOF coating on Type 316L stainless steel (serial number E316L255), and are shown in Figure 8. These measured transients are clearly and unambiguously indicative of a loss of passivity at the highest potential level. Since this Alloy C-22 coating was tested in the as-sprayed condition, a roughness factor must be applied to convert the *apparent* current density into the *actual* current density.

Current transients were measured at various levels of constant applied potential (100 to 736 mV vs. OCP) in seawater at 90°C, for an as-sprayed (unpolished) HVOF coating of SAM1651 (SAM7) on a Type 316L stainless steel (serial number E316L410), and are shown in Figure 9. These measured transients are indicative of good passive-film stability, which is comparable to that of wrought Alloy C-22. Since this as-sprayed SAM1651 (SAM7) coating was tested in the as-sprayed condition, a roughness factor must be applied to convert the *apparent* current density into the *actual* current density. From visual inspection, it was evident that passivity was maintained at higher potentials.

Potentiostatic Data – Concentrated Calcium Chloirde at 105°C

Potential-step testing has been performed on HVOF coatings of SAM1651 (SAM7) on Type 316L stainless steel (serial number E316L475) in extremely aggressive 5M CaCl$_2$ heated to 105°C, as shown in Figure 10. Tests were also performed on the reference material, Alloy C-22, in both wrought and thermally sprayed condition (serial numbers CC-22-4008 and E316L256, respectively). To eliminate the need for surface roughness corrections in the conversion of measured current and electrode area to current density, the SAM1651 (SAM7) coating was

polished to a 600-grit finish prior to testing. The curves represent the asymptotic current density reached after 24 hours at the corresponding potential. In this series of experiments, the passive film on wrought Alloy C-22 also commences breakdown at a potential of only 240 mV above the open circuit corrosion potential, with evidence of repassivation at potentials above 400 mV. Even with the repassivation at higher potential, the window of vulnerability between 240 to 400 mV is problematic for the reference material (Alloy C-22). Passive film breakdown on the HVOF coating of SAM1651 (SAM7) occurred at a significantly higher applied potential, between 360 and 400 mV, where breakdown of the passive film on thermally sprayed Alloy C-22 was virtually spontaneous. The new SAM1651 (SAM7) coating provides clear advantages for operation in hot concentrated chloride brines with aggressive divalent cations such as calcium.

Current transients wee measured at various levels of constant applied potential (100 to 450 mV vs. OCP) in 5M $CaCl_2$ at 105°C, for a polished SAM1651 (SAM7) HVOF coating on a Type 316L stainless steel (serial number E316L475), and are shown in Figure 11. These transients are indicative of good passive film stability, which is superior to that of wrought Alloy C-22 in this very aggressive environment. To eliminate the need for surface roughness corrections in the conversion of measured current and electrode area to current density, the SAM1651 (SAM7) coating was polished to a 600-grit finish prior to testing. Passive film breakdown on the HVOF coating of SAM1651 (SAM7) occurred at an applied potential between 360 and 400 mV vs. OCP, with a clear loss of passivity at 450 mV.

Current transients were measured at various levels of constant applied potential ranging (100 to 550 mV vs. OCP) in 5M $CaCl_2$ at 105°C, for wrought Alloy C-22 (serial number CC-22 4008), and are shown in Figure 12. These transients show complete breakdown of the passive film in two potential regimes, one regime located between 300-400 mV vs. OCP (350 mV), and the second located above 500 mV vs. OCP (550 mV). Like the polished SAM1651 (SAM7) coating, this reference was also polished to a 600-grit finish.

Current transients were measured at various levels of constant applied potential (100 to 350 mV vs. OCP) in 5M $CaCl_2$ at 105°C, for an as-sprayed (unpolished) Alloy C-22 HVOF coating on Type 316L stainless steel (serial number E316L256), and are shown in Figure 13. This as-sprayed HVOF coating of Alloy C-22 appears to be passive at 100-150 mV vs. OCP, but has a clear loss of passivity at potentials above 200 mV vs. OCP (250-350 mV).

Linear Polarization Data – Corrosion Rates

Linear polarization was used to determine the approximate corrosion rates of the thermal spray coatings of amorphous metals of interest (HVOF SAM1651 or SAM7 and other coatings) and the reference material (wrought nickel-based Alloy C-22) in three relevant environments, Seawater at two temperature levels, and in hot concentrated calcium chloride (5M $CaCl_2$ at 105°C). Values of the corrosion potential, polarization resistance, corrosion current density, and corrosion rate are summarized in Table 5 and Figure 14 through 16. In seawater at 30°C, the corrosion rates of HVOF SAM1651 (SAM7) coatings exhibited comparable to slightly higher corrosion rates than either wrought sample of Alloy C-22. As the temperature of the seawater was increased to 90°C, the corrosion rates of HVOF SAM1651 (SAM7) coatings exhibited comparable to slightly lower corrosion rates than either wrought sample of Alloy C-22. In general, corrosion rates trended to higher values with increasing temperature, as expected. In

calcium chloride at 105°C, the corrosion rates of HVOF SAM1651 (SAM7) coatings were slightly lower than that of HVOF Alloy C-22; and comparable to slightly greater than those of wrought Alloy C-22. In general, the corrosion rates observed in the hot calcium chloride (105°C) were higher than those observed in the heated seawater (90°C), which was also expected.

Salt Fog Testing – Verification of Corrosioin Resistance

As shown in Figure 17, salt fog testing was conducted on several thermal spray coatings, including HVOF coatings of Alloy C-22, Type 316L stainless steel, SAM40 (also referred to as DAR40), SAM1651 (SAM7) and other amorphous-metal formulations of interest. After 13 cycles in the GM9540P salt fog test, the HVOF coatings of Type 316L stainless steel and SAM40 showed substantial corrosion. Very slight rust spots were observed on the C-22 coating. In contrast, the newer SAM1651 (SAM7) formulations showed no corrosion at 30 cycles. The testing was continued to almost 60 cycles, with no evidence of corrosion observed with SAM1651 and other amorphous-metal formulations of interest.

CONCLUSIONS

SAM1651 has a low critical cooling rate (CCR), due to the addition of yttrium (Y), which enables it to be rendered as a completely amorphous thermal spray coating. The yttrium addition increases the viscosity of the alloy, thereby slowing the nucleation and growth kinetics of crystalline phases. Unfortunately, such increases in viscosity also make this material relatively difficult to gas atomize, with the powders having irregular shapes. Such non-spherical particle morphology causes pneumatic conveyance of the SAM1651 powder during thermal spray operations to be difficult. The production of nearly spherical gas-atomized SAM1651 powder with acceptable flow characteristics has required extensive particle sorting, exotic and expensive milling to eliminate irregularities, and significant process optimization.

The hypothesis that the corrosion resistance of Fe-based amorphous metals can be enhanced through application of heuristic principles related to the additions of chromium, molybdenum, tungsten and yttrium has been tested with SAM7 (SAM1651) and SAM8 formulations, and found to have merit. The decision to achieve enhanced corrosion resistance in these Fe-based amorphous metals was initially based upon two considerations. First, substantial enhancements in corrosion resistance had been observed in stainless steels and nickel based alloys by adding chromium, molybdenum, tungsten, as well as other alloying elements. Secondly, this enhancement in localized corrosion resistance can be quantified in the pitting resistance equivalence number, and could be used as a guide to determine the level of molybdenum addition necessary to achieve localized corrosion resistance comparable to nickel-based Alloy C-22, one of the benchmark materials. Electrochemical tests have been used to prove that corrosion performance comparable to nickel-based Alloy C-22 can be achieved with the new Fe-based amorphous metals in 5M CaCl2 at 105°C and seawater at 90°C.

Thermal spray coatings produced with early Fe-based amorphous metal formulations (SAM35, SAM40, and SAM40X3) had non-optimal elemental compositions, were produced with non-optimal thermal spray parameters (powder size, gun pressure, and particle velocity), and exhibited rusting after 13 cycles in the standardized salt fog tests. However, dense and pore-free thermal spray coatings produced with improved amorphous metal formulations that have greater

concentrations of chromium, molybdenum and yttrium (SAM7, also known as SAM1651) showed no corrosion after more than 30 cycles (and up to 54 cycles) in the salt fog test. Such performance cannot be achieved with thermally sprayed Type 316L stainless steel, as this material loses most of its desirable corrosion-resistance during the thermal spray process. To a lesser extent, similar difficulties are encountered during the thermal spraying of Alloy C-22.

The second hypothesis tested was that amorphous metals can have better corrosion resistance than comparable, crystalline materials. Ingots and melt-spun ribbons of the Fe-based SAM7 (SAM1651) and SAM8 amorphous metals, both free of grain boundaries, have shown much more resistance to corrosion (passive film stability) in aggressive environments such as 5M $CaCl_2$ at 105°C than crystalline Type 316L stainless steel and nickel-based Alloy C-22. It has also been found that it is not been possible to render Alloy C-22 as thermal spray coating with the same corrosion resistance as the wrought alloy, though such possibilities do exist with some of the Fe-based amorphous metal formulations discussed here. Corrosion resistance of Fe-based amorphous metals without yttrium additions, such as SAM2X5.

It has been shown that these novel ultra-hard corrosion-resistant materials can be produced as either bulk alloys or coatings. For example, melt spinning and arc melting with drop casting can be used to render these materials as fully dense pore-free bulk alloys. Coatings can be produced with advanced thermal spray processes, or by physical vapor deposition processes such as magnetron sputtering or electron-beam evaporation. The materials can also be rendered as bulk alloys by using HVOF to form large plates on a flat mandrel. Near theoretical density has been achieved through precise control of powder size with atomization and classification.

ACKNOWLEDGMENTS

REFERENCES

1. J. C. Farmer, J. J. Haslam, S. D. Day, T. Lian, R. Rebak, N. Yang, L. Aprigliano, Corrosion Resistance of Iron-Based Amorphous Metal Coatings, Proceedings of ASME PVP: Pressure Vessels & Piping (PVP) Division Conference, July 23-27, 2006 Vancouver, British Colombia, American Society of Mechanical Engineers, PVP2006-ICPVT11-93835, New York, NY 7 p. (2006).

2. J. C. Farmer, J. J. Haslam, S. D. Day, D. J. Branagan, C. A. Blue, J. D. K. Rivard, L. F. Aprigliano, N. Yang, J. H. Perepezko, M. B. Beardsley, Corrosion Characterization of Iron-Based High-Performance Amorphous-Metal Thermal-Spray Coatings, PVP2005-71664, Proceedings of ASME PVP: Pressure Vessels & Piping Division Conference, Grand Hyatt, Denver, Colorado, July 17-21, 2005, American Society of Mechanical Engineers, Three Park Avenue, New York, New York, 7 pages (2005).

3. J. C. Farmer, J. J. Haslam, S. D. Day, D. J. Branagan, M. C. Marshall, B. E. Mecham, E. J. Buffa, C. A. Bue, J. D. K. Rivard, D. C. Harper, M. B. Beardsley, D. T. Weaver, L. F. Aprigliano, L. Kohler, R. Bayles, E. J. Lemieux, T. M. Wolejsza, N. Yang, G. Lucadamo, J. H. Perepezko, K. Hildal, L. Kaufman, A. H. Heuere, F. Ernst, G. M. Michal, H. Kahn, E. J. Lavernia, High-Performance Corrosion-Resistant Materials: Iron-Based Amorphous-Metal Thermal-Spray Coatings, High-Performance Corrosion-Resistant Materials (HPCRM) Annual Report, UCRL-TR-206717, Lawrence Livermore National Laboratory, Livermore, California, 178 pages, September 28 (2004).

4. F. Guo, S. J. Poon, G. J. Shiflet, Metallic Glass Ingots Based on Yttrium, Applied Physics Letters, Vol. 83, No. 13, pp. 2575-2577 (2003).

5. Z. P. Lu, C. T. Liu, W. D. Porter, Role of Yttrium in Glass Formation of Fe-Based Bulk Metallic Glasses, Vol. 83, No. 13, Applied Physics Letters, pp. 2581-2583 (2003).

6. V. Ponnambalam, S. J. Poon and G. Shiflet, J. Mater. Res., 19 (5), 1320, 2004.

7. D. J. Branagan, M. C. Marshall, B. E. Mecham, L. F. Aprigliano, R. Bayles, E. J. Lemieux, T. M. Wolejsza, F. J. Martin, J. C. Farmer, J. J. Haslam, S. D. Day, Wear and Corrosion Resistant Amorphous / Nanostructured Steel Coatings for Replacement of Electrolytic Hard Chromium, UCRL Report, Lawrence Livermore National Laboratory, Livermore, California. 7 pages (2005); Proceedings of the International Thermal Spray Conference and Exposition, American Society of Materials International, Seattle, Washington, May 15-18, 2006 (2006).

8. D. J. Branagan, Method of Modifying Iron-Based Glasses to Increase Crystallization Temperature without Changing Melting Temperature, United States Patent Application No. 20040250929, Filed December 16, 2004.

9. D. J. Branagan, Properties of Amorphous/Partially Crystalline Coatings, United States Patent Application No. 20040253381, Filed December 16, 2004.

10. D. J. Branagan, Methods of Forming Hardened Surfaces, United States Patent No. 6,767,419, Filed November 9, 2000, Granted July 27, 2004.

11. D. J. Branagan, Method for Protecting a Surface, United States Patent Application 20040140021, Filed July 22, 2004.

12. D. J. Branagan, Joseph V. Burch, Methods of Forming Steel, United States Patent No. 6,258,185, Filed May 25, 1999, Granted July 10, 2001.

13. D. Chidambaram, C. R. Clayton, M. R. Dorfman, Evaluation of the Electrochemical Behavior of HVOF-Sprayed Alloy Coatings, Surface and Coatings Technology, Vol. 176, pp. 307-317 (2004).

14. D. E. Polk, B. C. Giessen, Overview of Principles and Applications, Chapter 1, pp. 2-35, Metallic Glasses, J. J. Gilman, H. J. Leamy, Eds., American Society of Metals, Metals Park, Ohio, 348 p. (1978).

15. R. M. Latanison, Corrosion Resistance of Metastable Alloys Processed by Rapid Solidification, Workshop on Amorphous Metals and Semiconductors, Electric Power Research Institute (EPRI), May 12-18, 1985 (1985).

16. J. R. Scully, A. Gerbert, J. H. Payer, Corrosion and Related Mechanical Properties of Bulk Metallic Glasses, Journal of Materials Research, submitted for publication (2006).

17. K. Kishitake, H. Era, F. Otsubo, Characterization of Plasma Sprayed Fe-10Cr-10Mo-(C,B) Amorphous Coatings, Vol. 5, No. 2, pp. 145-153 (1996).

18. S. Pang, T. Zhang, K. Asami, A. Inoue, Materials Transactions, Effects of Chromium on the Glass Formation and Corrosion Behavior of Bulk Glassy Fe-Cr-Mo-C-B Alloys, Vol. 43, No. 8, pp. 2137-2142 (2002).

19. S. J. Pang, T. Zhang, K. Asami, A. Inoue, Synthesis of Fe-Cr-Mo-C-B-P Bulk Metallic Glasses with High Corrosion Resistance, Acta Materialia, Vol. 50, pp. 489-497 (2002).

20. H. Shinimiya, A. Nakazawa, Z. Kato, A. A. El Moneium, Y. Niizeki, K. Asami, K. Hashimoto, Corrosion Resistant Bulk Amrophous Ni-Cr-Ta-Mo-Nb-5P Alloys in Concentrated Hydrochloric Acids, Paper 319, Session on Corrosion and Electrochemistry of Advanced Materials in Honor of Koji Hashimoto, 208th Meeting of the Electrochemical Society, Westing Bonaventure Hotel, Los Angeles, California, October 16-21, 2005, Electrochemical Society, Pennington, New Jersey (2005).

21. J. E. Harrar, J. F. Carley, W. F. Isherwood, E. Raber, Report of the Committee to Review the Use of J-13 Well Water in Nevada Nuclear Waste Storage Investigations, Yucca Mountain Project, UCID-21867, Lawrence Livermore National Laboratory, Livermore, California, 111 pages (1990).

22. H. P. Hack, Crevice Corrosion Behavior of Molybdenum-Containing Stainless Steel in Seawater, Materials Performance, Vol. 22, No. 6, pp. 24–30 (1983).

23. K. A. Gruss, G. A. Cragnolino, D. S. Dunn, N. Sridar, Repassivation Potential for Localized Corrosion of Alloys 625 and C22 in Simulated Repository Environments, Paper 149, Corrosion 98, National Association of Corrosion Engineers, Houston, TX, 9 pages (1998).

24. A. I. Asphahani, Corrosion Resistance of High Performance Alloys, Materials Performance, Vol. 19, No. 12, pp. 33–43 (1980).

25. C. K. Saw, X-ray Scattering Techniques for Characterization Tools in the Life Sciences, Nanotechnologies for the Life Science, Edited by Challa Kumar, Wiley-VCH Verlag GmbH & Co., KGaA, Weinheim (2006).

26. C. K. Saw and R. B. Schwarz, Chemical Short-Range Order in Dense Random-Packed Models", Journal of the Less-Common Metals, 140, 385-393 (1988).

27. J. R. Scully, J. L. Hudson, T. Lunt, G. Ilevbare, B. Kehler, Localized Corrosion Initiation and Transition to Stabilization in Alloys 625 and C-22, Final Report, TRW/DOE YMP Purchase Order Number A10762JM8A, September 30, 1999, 27 pages (1999).

28. Standard Practice for Conventions Applicable to Electrochemical Measurements in Corrosion Testing, Designation G 3-89, 1997 Annual Book of American Society for Testing and Materials (ASTM) Standards, Section 3, Vol. 3.02, pp. 36–44 (1997).

29. Standard Reference Test Method for Making Potentiostatic and Potentiodynamic Anodic Polarization Measurements, Designation G 5-94, 1997 Annual Book of American Society for Testing and Materials (ASTM) Standards, Section 3, Vol. 3.02, pp. 54–57 (1997).

30. Standard Reference Test Method for Making Potentiostatic and Potentiodynamic Anodic Polarization Measurements, Designation G 5-87, 1989 Annual Book of American Society for Testing and Materials (ASTM) Standards, Section 3, Vol. 3.02, pp. 79–85 (1989).

31. Standard Test Method for conducting Cyclic Potentiodynamic Polarization Measurements for Localized Corrosion Susceptibility of Iron-, Nickel-, or Cobalt-Based Alloys, Designation G 61-86, 1997 Annual Book of American Society for Testing and Materials Standards, Section 3, Vol. 3.02, pp. 231–235 (1997).

32. W. T. Kim, K. Clay, C. Small, B. Cantor, Heat Treatment of a Melt Spun Fe70Cr18Mo2B10 Alloy, Journal of Non-Crystalline Solids, Vol. 127, pp. 273-286 (1991).

33. R. S. Treseder, R. Baboian, C. G. Munger, Polarization Resistance Method for Determining Corrosion Rates, NACE Corrosion Engineer's Reference Book, Second Edition, National Association of Corrosion Engineers, 1440 South Creek Drive, Houston, Texas, pp. 65-66 (1991).

34. D. A. Jones, Faraday's Law, Section 3.1.1, Electrochemical Kinetics of Corrosion," Chapter 3, Principles and Prevention of Corrosion, 2nd Edition, Prentice Hall, Upper Saddle River, NJ, Equations 3 and 5, pp. 75–76 (1996).

35. A. J. Bard, L. R. Faulkner, Liquid Junction Potentials, Section 2.3, Potentials and Thermodynamics of Cells, Chapter 2, Electrochemical Methods, Fundamentals and Applications, John Wiley and Sons, New York, NY, 1980, Eqn. 2.3.39, p. 71, Table 2.3.2, p. 67 (1980).

TABLES

Table 1 – The melt-spinning process was used to perform a systematic study of various elemental compositions, each based on the Fe-based DAR40 composition, with 1, 3, 5, and 7 atomic percent additions of specific elements believed to be beneficial to glass formation or corrosion resistance. Elemental additions investigated included nickel (Ni), molybdenum (Mo), yttrium (Y), titanium (Ti), zirconium (Zr) and chromium (Cr). The two formulations of greatest interest at the present time, based upon corrosion resistance and ease of processing are SAM2X5 ($Fe_{49.7}Cr_{17.7}Mn_{1.9}Mo_{7.4}W_{1.6}B_{15.2}C_{3.8}Si_{2.4}$), which has a relatively high CCR, and yttrium-containing SAM1651 (SAM7) or SAM7 ($Fe_{48.0}Cr_{15.0}Mo_{14.0}B_{6.0}C_{15.0}Y_{2.0}$), which has a relatively low CCR.

Nominal Composition in Atomic Percent - Used to Prepare Samples														
Alloy	Specification / Formula	Fe	Cr	Mn	Mo	W	B*	C*	Si	Y	Ni	P*	Co	Total
316L	UNS S31603	68.0	18.0	1.5	1.5	0.0	0.0	0.0	1.0	0.0	10.0	0.0	0.0	100
C-22	UNS N06022	4.0	25.0	0.1	8.0	1.4	0.0	0.0	1.0	0.0	60.0	0.0	0.5	100
SAM40	$Fe_{52.3}Mn_2Cr_{19}Mo_{2.5}W_{1.7}B_{16}C_4Si_{2.5}$	52.3	19.0	2.0	2.5	1.7	16.0	4.0	2.5	0.0	0.0	0.0	0.0	100
SAM3X1	$(DAR40)_{99} + Y_1$	51.8	18.8	2.0	2.5	1.7	15.8	4.0	2.5	1.0	0.0	0.0	0.0	100
SAM3X3	$(DAR40)_{97} + Y_3$	50.7	18.4	1.9	2.4	1.6	15.5	3.9	2.4	3.0	0.0	0.0	0.0	100
SAM3X5	$(DAR40)_{95} + Y_5$	49.7	18.1	1.9	2.4	1.6	15.2	3.8	2.4	5.0	0.0	0.0	0.0	100
SAM3X7	$(DAR40)_{93} + Y_7$	48.6	17.7	1.9	2.3	1.6	14.9	3.7	2.3	7.0	0.0	0.0	0.0	100
SAM1651	$Fe_{48}Mo_{14}Cr_{15}Y_2C_{15}B_6$	48.0	15.0	0.0	14.0	0.0	6.0	15.0	0.0	2.0	0.0	0.0	0.0	100

Table 2 – The actual compositions of several samples used in this study were determined with energy dispersive X-ray spectroscopy (EDS), and are summarized here. The measurements were done for wrought samples of Type 316L stainless steel and nickel-based Alloy C-22; melt-spun ribbons of SAM40, SAM2X1, SAM2X3, SAM2X5 and SAM2X7; and a drop-cast SAM1651 (SAM7) ingot. Attempts to produce melt spur ribbons of SAM7 resulted in a final composition of only 0.2 atomic percent yttrium.

Actual Compositions in Atomic Percent - Determined by Energy Dispersive X-Ray Spectroscopy														
Alloy	Specification / Formula	Fe	Cr	Mn	Mo	W	B*	C*	Si	Y	Ni	P*	Co	Total
316L	UNS S31603	67.6	18.7	1.3	1.2	0.0	0.0	0.0	1.2	0.0	10.0	0.0	0.0	100
C-22	UNS N06022	3.9	25.2	0.1	7.8	1.4	0.0	0.0	1.1	0.0	60.0	0.0	0.5	100
SAM40	$Fe_{52.3}Mn_2Cr_{19}Mo_{2.5}W_{1.7}B_{16}C_4Si_{2.5}$	51.9	19.2	2.6	2.5	1.5	16.0	4.0	2.2	0.0	0.0	0.0	0.0	100
SAM3X1	$(DAR40)_{99} + Y_1$	49.1	19.2	1.8	3.1	3.0	15.8	4.0	2.9	1.0	0.0	0.0	0.0	100
SAM3X3	$(DAR40)_{97} + Y_3$	49.4	18.9	1.7	3.0	2.8	15.5	3.9	1.9	2.9	0.0	0.0	0.0	100
SAM3X5	$(DAR40)_{95} + Y_5$	48.8	18.4	1.5	2.6	2.6	15.2	3.8	2.2	4.8	0.0	0.0	0.0	100
SAM3X7	$(DAR40)_{93} + Y_7$	47.3	17.8	2.1	2.5	2.6	14.9	3.7	2.2	6.8	0.0	0.0	0.0	100
SAM1651	$Fe_{48}Mo_{14}Cr_{15}Y_2C_{15}B_6$	49.1	14.6	0.0	13.9	0.0	5.9	14.0	0.3	1.9	0.2	0.0	0.0	100

Table 3 – Thermal analysis data (DTA or DSC) for Fe-based glass forming alloys suitable for thermal spray deposition as summarized in this table. The two formulations of greatest interest at the present time are SAM2X5 ($Fe_{49.7}Cr_{17.7}Mn_{1.9}Mo_{7.4}W_{1.6}B_{15.2}C_{3.8}Si_{2.4}$), which has a relatively high CCR, and yttrium-containing SAM1651 (SAM7) or SAM7 ($Fe_{48.0}Cr_{15.0}Mo_{14.0}B_{6.0}C_{15.0}Y_{2.0}$), which has a relatively low CCR. These selections are based upon their good corrosion resistance and relative ease or processing.

Alloy	T_g (°C)	T_x (°C)	T_m (°C)	T_L (°C)	T_{rg}
SAM40	568-574	623	1110	1338	0.53
SAM3X1	560	614	1108	min. 1320	0.52
SAM3X3	573	659	1138	min. 1380	0.51
SAM3X5	590	677	1143	min. 1400	0.52
SAM3X7	not clear	697	1164	min. 1420	
SAM1651	584	653	1121	1290	0.55

Table 4 – The hardness (kg mm^{-2}) for as-sprayed SAM1651 HVOF coatings is summarized here.

HV100								
Indentation	**HV1**	**HV2**	**HV3**	**HV4**	**HV5**	**HV6**	**HV7**	**HV8**	**HV9**
1	1046	1191	840	1232	1097	955	1048	1183	931
2	1129	1103	1181	1175	1121	988	1202	1140	903
3	1004	1022	978	1130	979	1089	1155	1035	827
4	861	1059	1104	1033	1120	1075	1160	1105	893
5	883	1115	1154	1075	1043	975	1205	1058	979
Average	985	1098	1051	1129	1072	1016	1154	1104	907
Std. Dev.	112	64	142	79	61	61	64	60	56
HV300								
Indentation	**HV1**	**HV2**	**HV3**	**HV4**	**HV5**	**HV1**	**HV2**	**HV3**	**HV4**
1	919	994	910	985	894	987	992	908	856
2	789	1038	889	861	876	870	1058	1024	908
3	784	1005	848	848	887	944	965	1050	921
4	892	1004	1011	977	886	837	970	911	880
5	901	943	854	810	917	876	971	924	894
Average	857	997	902	896	892	903	991	963	892
Std. Dev.	65	34	66	80	15	61	39	68	25

Table 5 – The conversion of the corrosion current density to penetration rate (corrosion rate) requires the parameters summarized in this table. These penetration rates are for an assumed current density of one microamp per square centimeter (1 μA cm^{-2}). If the corrosion rate is 2 μA cm^{-2} instead of the assumed 1 μA cm^{-2}, the penetration rate is simply doubled. The value of Faraday's constant (F) is 96,484.6 C equiv^{-1}.

Alloy	ρ_{alloy}	$n_{alloy} = (f_j n_j/a_j)/100$		$(dp/dt) = (i_{corr})/(\rho_{alloy} \times n_{alloy} \times F)$			
	g cm^{-3}			cm sec^{-1}		μm year^{-1}	
		Low	High	Low	High	Low	High
316L SS	7.85	3.9049E-02	6.5291E-02	2.0222E-11	3.3811E-11	6.3772	10.6627
C-22	8.69	3.8041E-02	6.7509E-02	1.7667E-11	3.1352E-11	5.5714	9.8872
SAM2X5	7.65	5.4149E-02	7.9309E-02	1.7083E-11	2.5020E-11	5.3872	7.8904
SAM1651	6.18	4.6979E-02	8.0221E-02	2.0906E-11	3.5699E-11	6.5928	11.2579

Table 6 – Values of the polarization resistance, corrosion current density, and corrosion rate, measured with linear polarization, are summarized for HVOF coatings of SAM1651 and Alloy C-22, as well as wrought samples of Alloy C-22. Values of the open circuit corrosion potential are also presented.

Sample	Parameter	E_{corr}	R_p	i_{corr}	dp/dt
		mV	ohms cm²	A/cm²	µm/yr
30°C Seawater					
HVOF SAM1651	Average	-73.4	8.352E+05	3.56E-08	0.4004
HVOF SAM1651	Standard Deviation	4.1	4.672E+05	1.51E-08	0.1705
Wrought Alloy C-22	Average	-163.2	2.744E+06	9.12E-09	0.0901
Wrought Alloy C-22	Standard Deviation	1.5	9.126E+04	3.02E-10	0.0030
Wrought Alloy C-22	Average	-312.4	6.229E+07	5.07E-09	0.0501
Wrought Alloy C-22	Standard Deviation	3.0	1.020E+08	4.40E-09	0.0435
90°C Seawater					
HVOF SAM1651	Average	-227.8	1.761E+05	1.42E-07	1.599
HVOF SAM1651	Standard Deviation	3.0	6.150E+03	5.05E-09	0.057
Wrought Alloy C-22	Average	-318.9	7.685E+04	3.25E-07	3.216
Wrought Alloy C-22	Standard Deviation	0.8	4.950E+02	2.10E-09	0.021
Wrought Alloy C-22	Average	-340.1	7.727E+04	3.24E-07	3.199
Wrought Alloy C-22	Standard Deviation	0.2	1.030E+03	4.29E-09	0.042
Wrought Alloy C-22	Average	-318.2	2.033E+05	1.23E-07	1.216
Wrought Alloy C-22	Standard Deviation	0.7	9.074E+02	5.50E-10	0.005
105°C 5M CaCl₂					
HVOF SAM1651	Average	-292.6	2.81E+04	8.91E-07	10.027
HVOF SAM1651	Standard Deviation	4.6	2.49E+02	7.92E-09	0.089
Wrought Alloy C-22	Average	-464.3	4.93E+04	5.10E-07	5.040
Wrought Alloy C-22	Standard Deviation	3.0	4.14E+03	4.37E-08	0.433
HVOF Alloy C-22	Average	-347.9	2.14E+03	1.17E-05	115.692
HVOF Alloy C-22	Standard Deviation	4.5	8.94E+01	4.82E-07	4.770

Table 7 – A description of GM9540P Salt Fog Test is summarized here. Note that the salt solution mists (denoted with asterisks) consisted of 1.25% solution containing 0.9% sodium chloride, 0.1% calcium chloride, and 0.25% sodium bicarbonate.

24-Hour Test Cycle for GM9540P Accelerated Corrosion Test		
Shift	**Elapsed Time (hrs)**	**Event**
Ambient Soak	0	Salt solution mist for 30 seconds, followed by ambient exposure at 13-28°C (55-82°F)
	1.5	Salt solution mist for 30 seconds, followed by ambient exposure at 13-28°C (55-82°F)
	3	Salt solution mist for 30 seconds, followed by ambient exposure at 13-28°C (55-82°F)
	4.5	Salt solution mist for 30 seconds, followed by ambient exposure at 13-28°C (55-82°F)
Wet Soak	8 to 16	High humidity exposure for 8 hours at 49 ± 0.5°C (120 ± 1°F) and 100% RH, including a 55-minute ramp to wet conditions
Dry Soak	16 to 24	Elevated dry exposure for 8 hours at 60 ± 0.5°C (140 ± 1°F) and less than 30% RH, including a 175-minute ramp to dry conditions

FIGURES
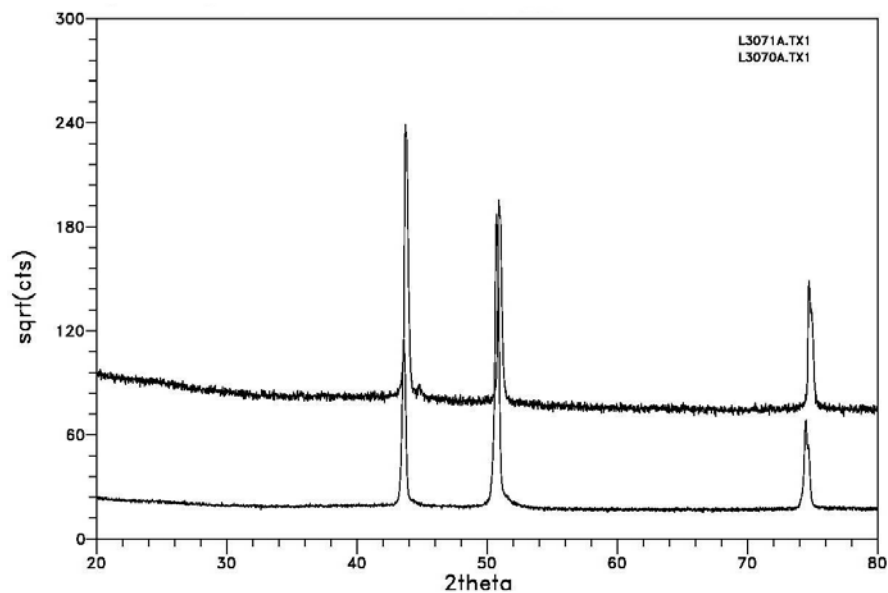
Figure 1 – This figure shows X-ray diffraction data for melt-spun ribbon (MSR) samples of Type 316L stainless steel and nickel-based Alloy C-22. The strong peaks are indicative of the crystalline nature of these materials.
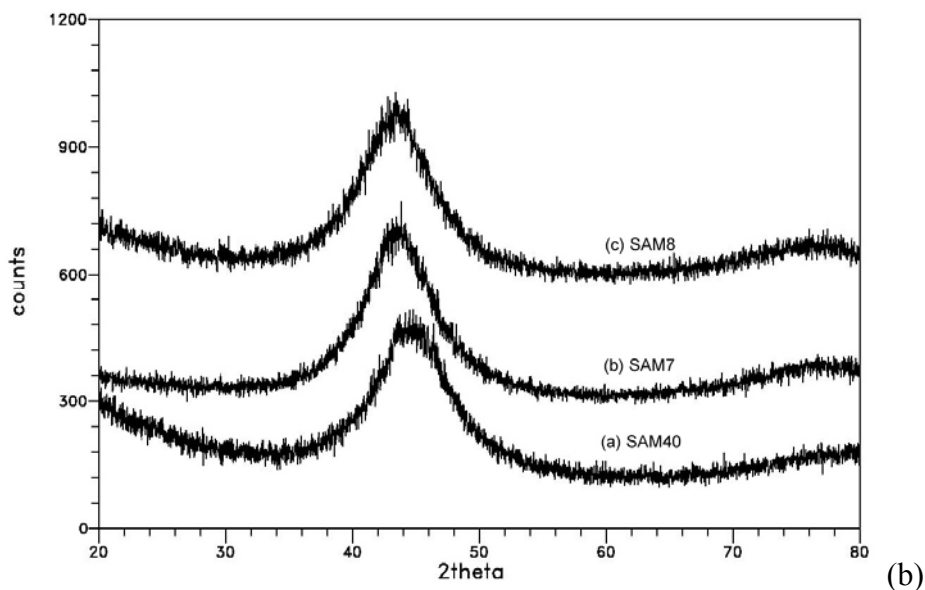
Figure 2 – This figure shows X-ray diffraction data for melt-spun ribbon (MSR) samples of iron-based amorphous metals identified as: (a) SAM40; (b) SAM7, which is also known as SAM1651; and (c) SAM8. These MSR samples are completely amorphous.

Corrosion Resistance of SAM1651 Ingot (Melt #19643)
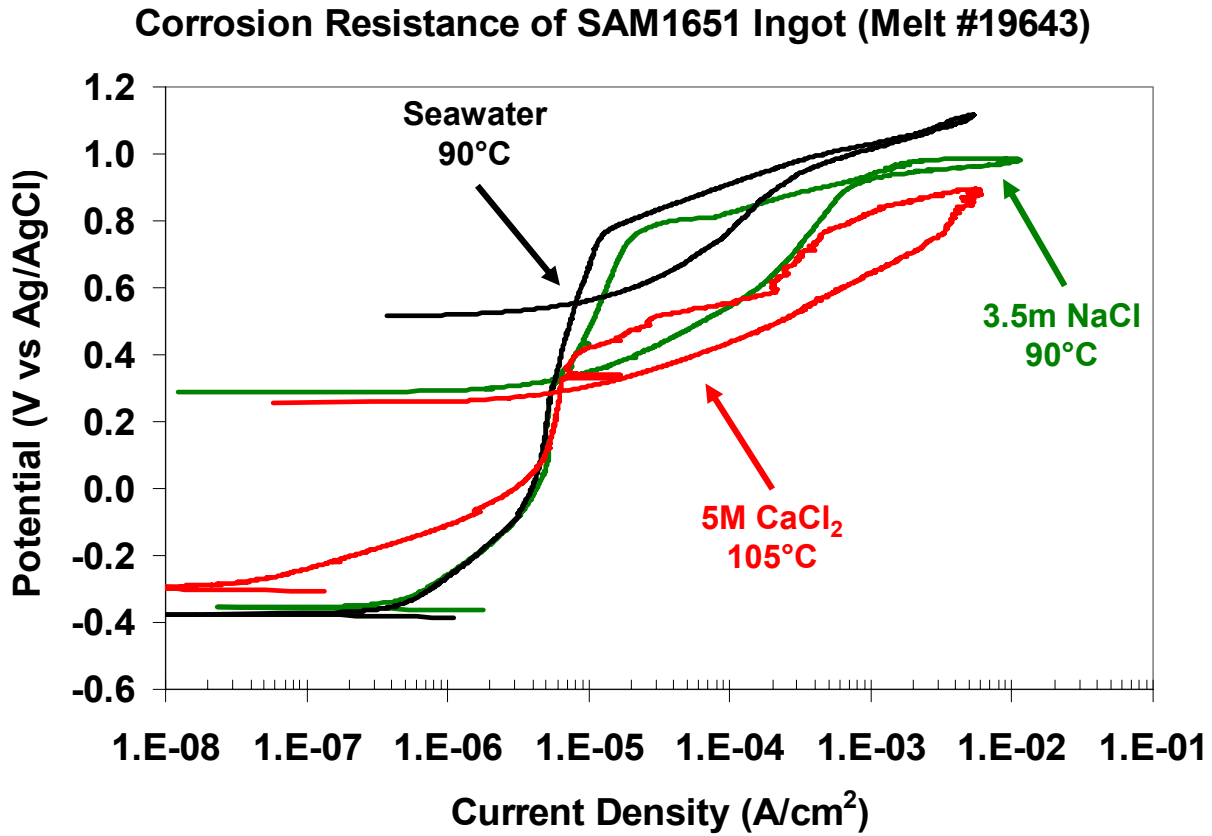
Figure 3 – Cyclic polarization data for three drop-cast ingots of SAM1651 (SAM7) Fe-based amorphous metal with yttrium in three different environments: seawater at 90°C; 3.5 molal NaCl at 90°C; and 5M CaCl₂ at 105°C. All three cyclic polarization curves show outstanding passivity.
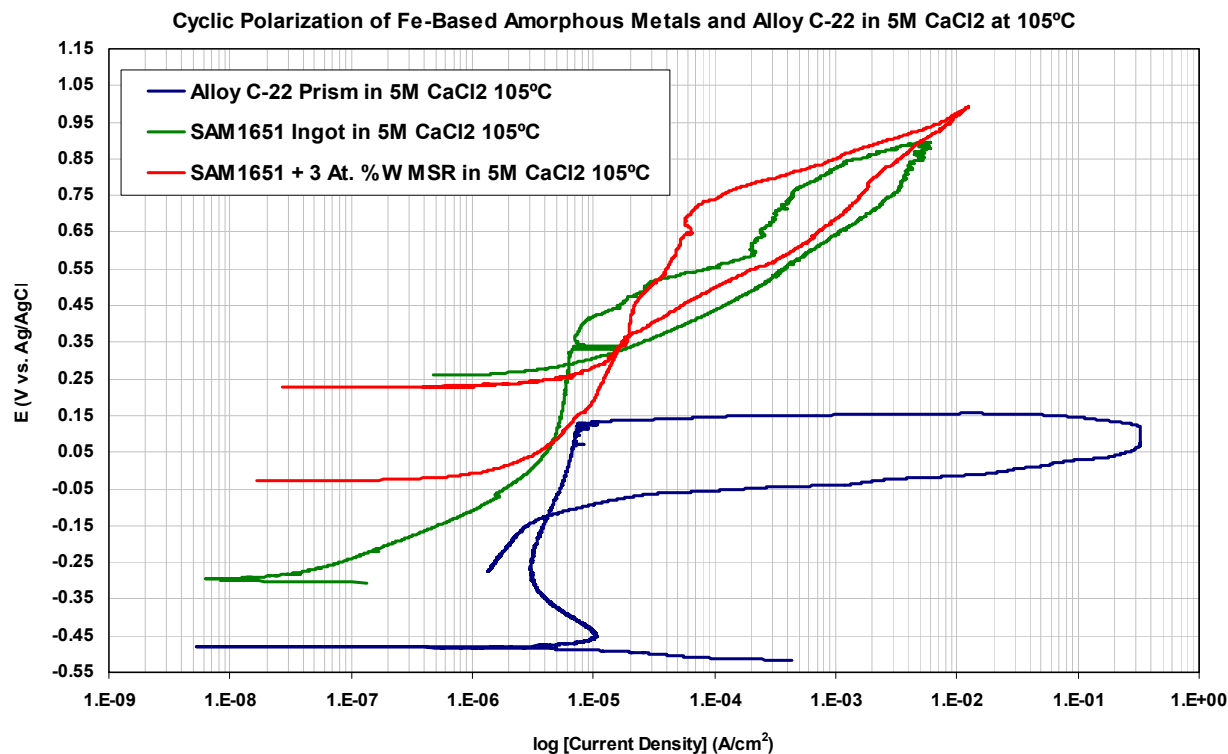
Figure 4 – Cyclic polarization data for a wrought prism of nickel-based Alloy C-22, a drop-cast ingot of iron-based SAM7 (SAM1651) amorphous metal, and a melt-spun ribbon of SAM8 (SAM1651 (SAM7) + 3 atomic percent tungsten), all obtained with 5M CaCl$_2$ at 105°C. Both the SAM7 and SAM8 showed passive film stability comparable to (or better than) Alloy C-22. The addition of 3 atomic-percent tungsten to the SAM1651 (SAM7) enhanced the passive film stability, and also yielded more ductile and damage-tolerant amorphous metal ribbons.

**Final Current Density vs. Applied Potential for
600-Grit Polished HVOF SAM1651, HVOF C-22 &
Wrought C-22 in Seawater at 90°C**
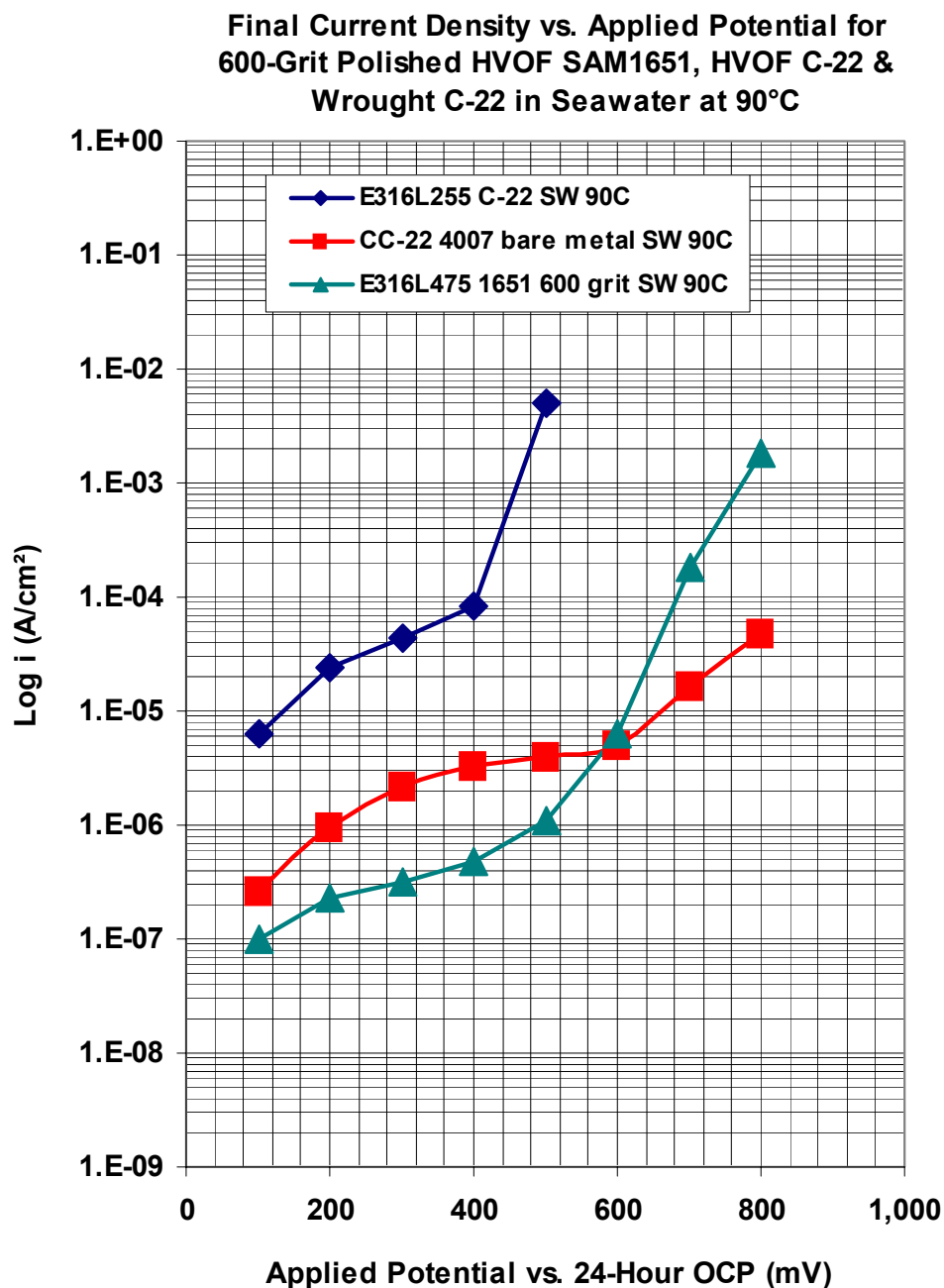
Figure 5 – Potential-step testing in deaerated seawater heated to 90°C has been performed with SAM1651 (SAM7) and Alloy C-22 thermal spray coatings, as well as wrought Alloy C-22. To eliminate the need for surface roughness corrections in the conversion of measured current and electrode area to current density, the SAM1651 (SAM7) coating was polished to a 600-grit finish prior to testing.
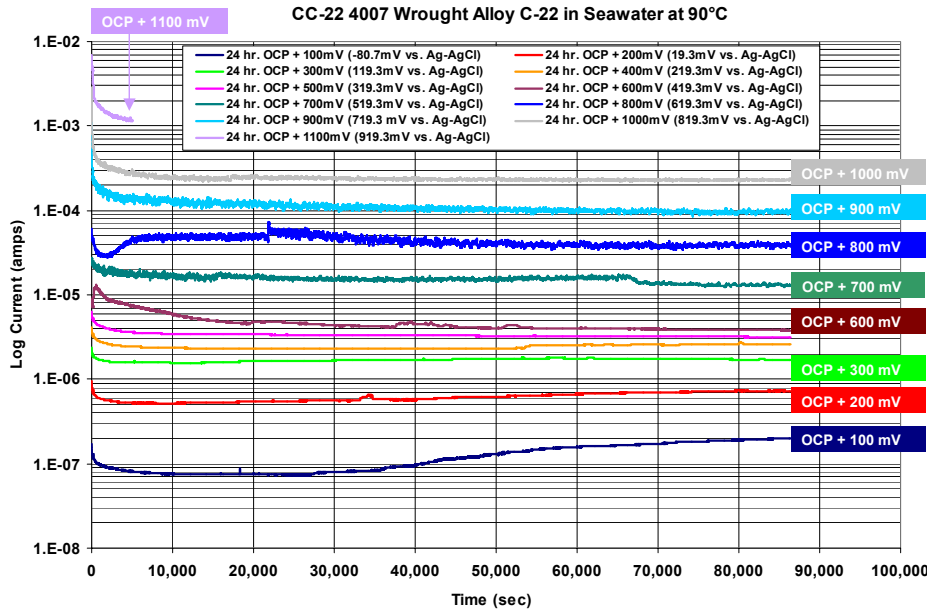
Figure 6 – Current transients at various levels of constant applied potential ranging from (100 to 1000 mV vs. OCP) in deaerated seawater at 90°C, for wrought nickel-based Alloy C-22 (serial number CC-22 4007).
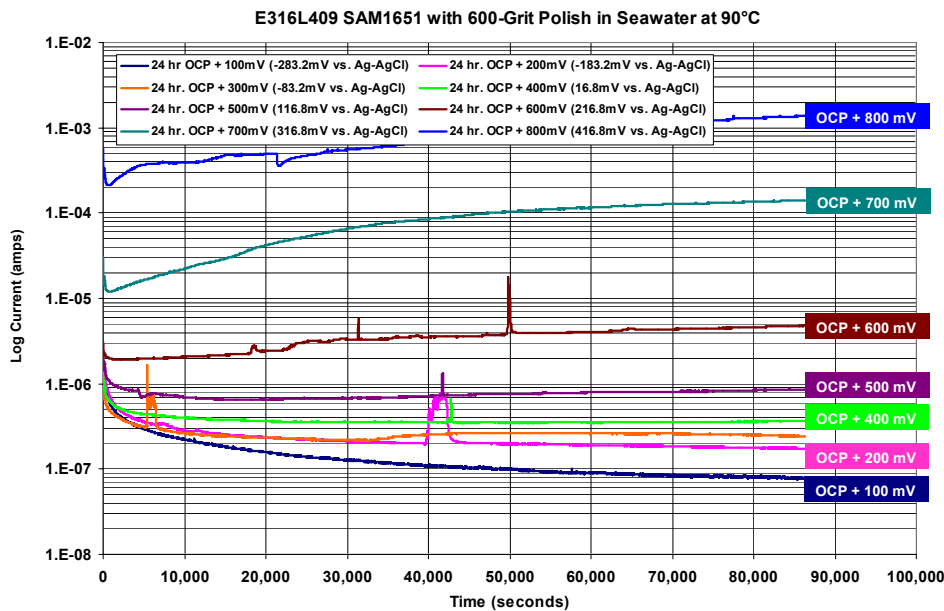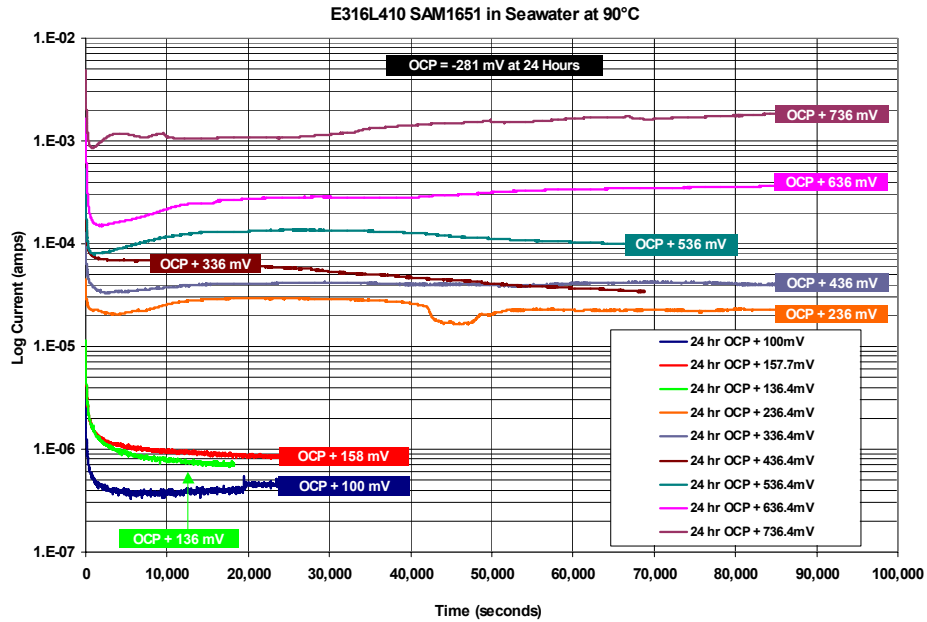

Figure 7 – Current transients were measured at various levels of constant applied potential (100 to 800 mV vs. OCP) in seawater at 90°C for a 600-grit polished SAM1651 (SAM7) HVOF coating on Type 316L stainless steel (serial number E316L409).
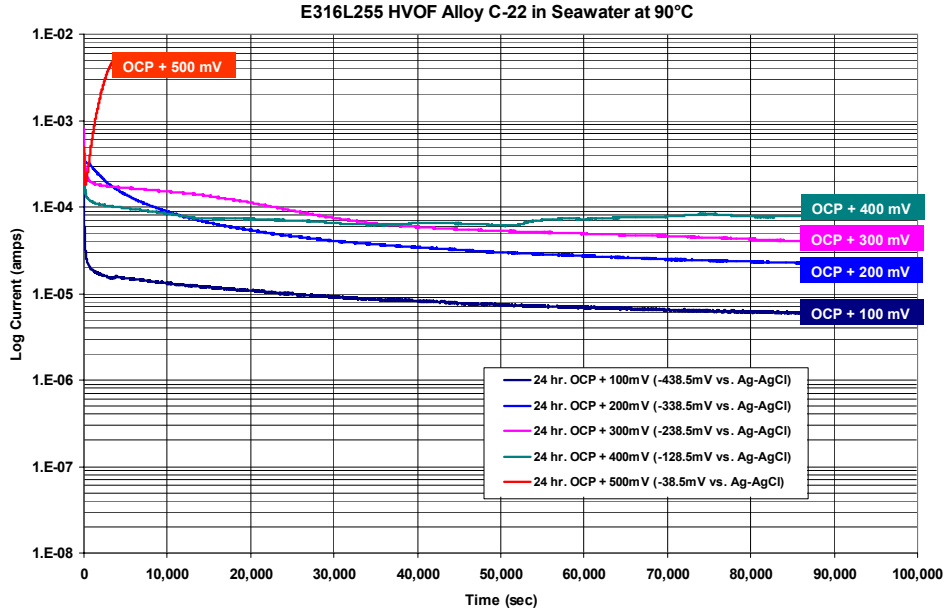
Figure 8 – Current transients were measured at various levels of constant applied potential (100 to 500 mV vs. OCP) in seawater at 90°C, for an as-sprayed (unpolished) Alloy C-22 HVOF coating on Type 316L stainless steel (serial number E316L255).
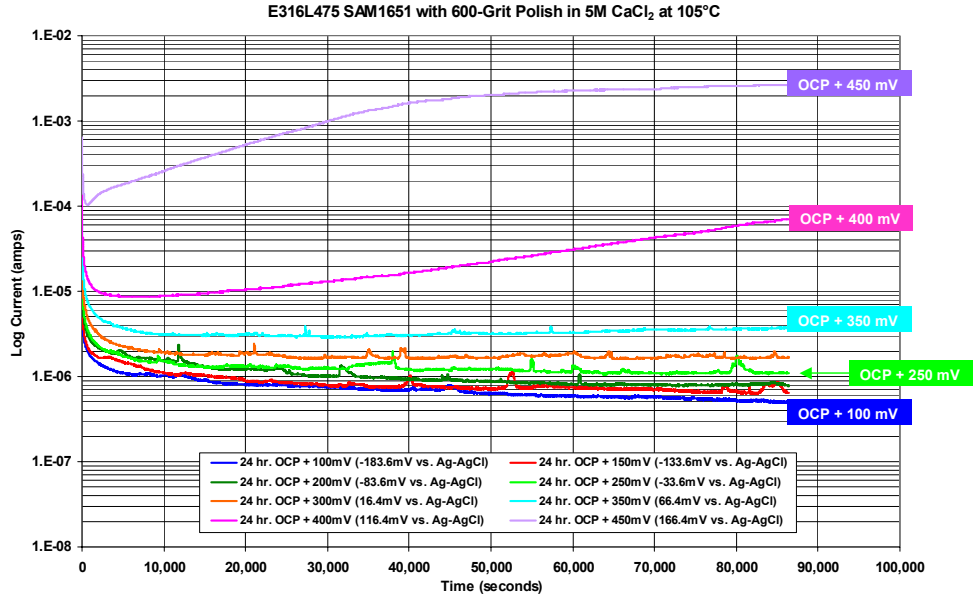

Figure 9 – Current transients were measured at various levels of constant applied potential (100 to 736 mV vs. OCP) in seawater at 90°C, for an as-sprayed (unpolished) HVOF coating of SAM1651 (SAM7) on a Type 316L stainless steel (serial number E316L410).

Figure 10 – Potential-step testing has been performed on HVOF coatings of SAM1651 (SAM7) on Type 316L stainless steel (serial number E316L475) in extremely aggressive 5M CaCl$_2$ heated to 105°C. Tests were also performed on the reference material, Alloy C-22, in both wrought and thermally sprayed condition (serial numbers CC-22-4008 and E316L256, respectively). To eliminate the need for surface roughness corrections in the conversion of measured current and electrode area to current density, the SAM1651 (SAM7) coating was polished to a 600-grit finish prior to testing.

E316L475 SAM1651 with 600-Grit Polish in 5M CaCl₂ at 105°C

Figure 11 – Current transients wee measured at various levels of constant applied potential (100 to 450 mV vs. OCP) in 5M CaCl$_2$ at 105°C, for a polished SAM1651 (SAM7) HVOF coating on a Type 316L stainless steel (serial number E316L475).
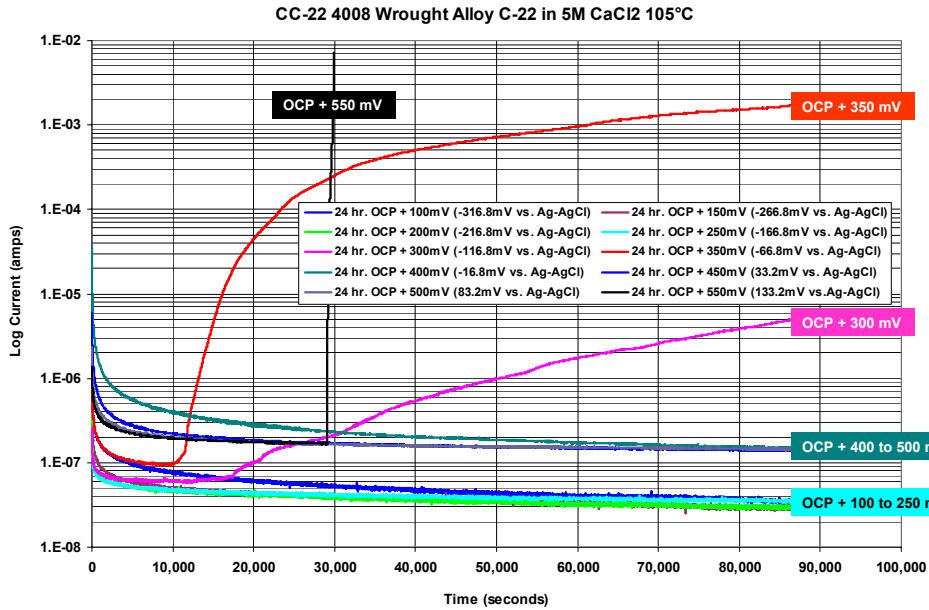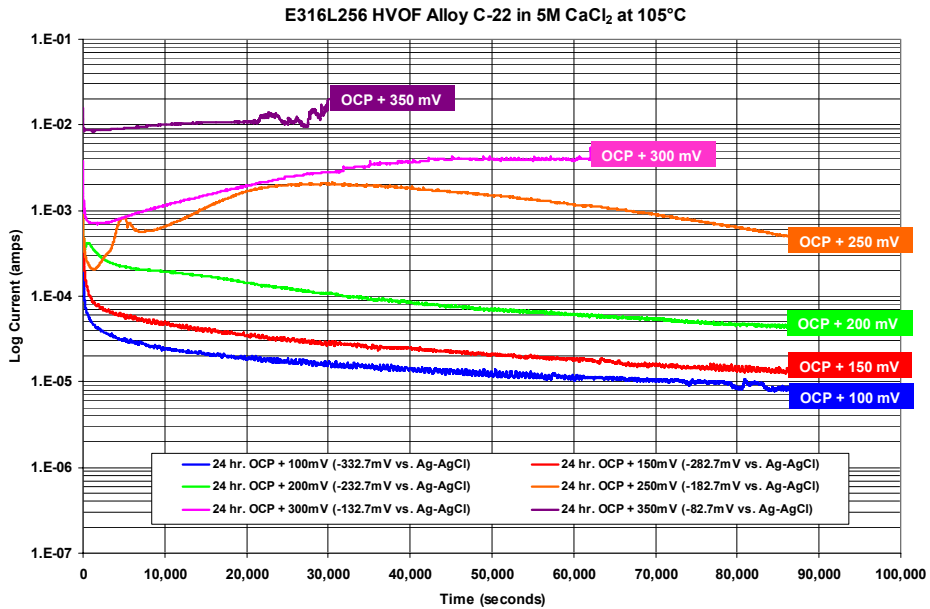
CC-22 4008 Wrought Alloy C-22 in 5M CaCl2 105°C

Figure 12 – Current transients were measured at various levels of constant applied potential ranging (100 to 550 mV vs. OCP) in 5M CaCl$_2$ at 105°C, for wrought Alloy C-22 (serial number CC-22 4008).

.

Figure 13 – Current transients were measured at various levels of constant applied potential (100 to 350 mV vs. OCP) in 5M $CaCl_2$ at 105°C, for an as-sprayed (unpolished) Alloy C-22 HVOF coating on Type 316L stainless steel (serial number E316L256).
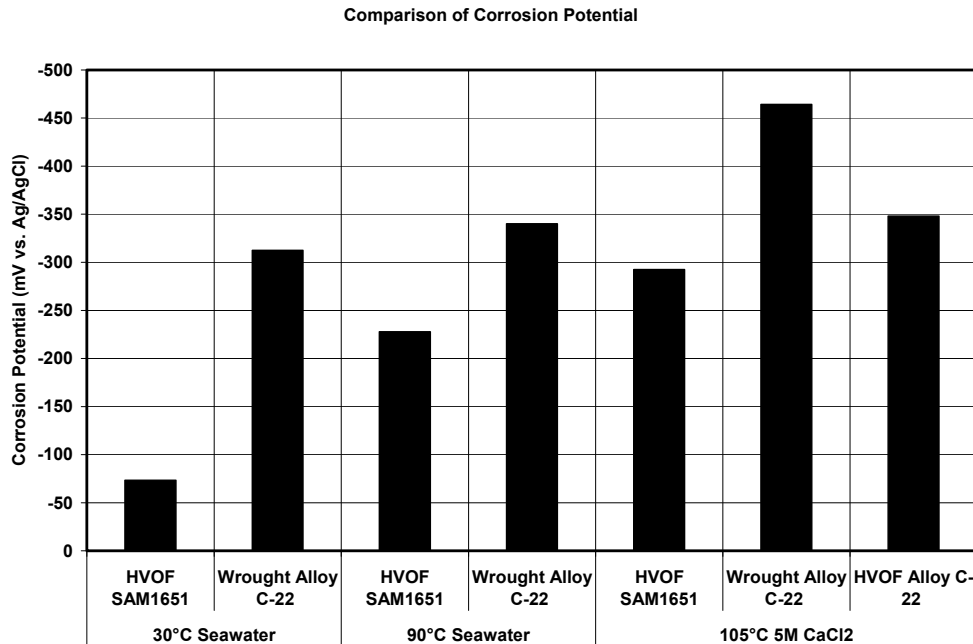

Figure 14 – The corrosion potentials for the thermal spray coatings of SAM1651 and the reference material (wrought nickel-based Alloy C-22) in three relevant environments, Half Moon Bay seawater at two temperature levels, and in hot concentrated calcium chloride (5M $CaCl_2$ at 105°C) are summarized.

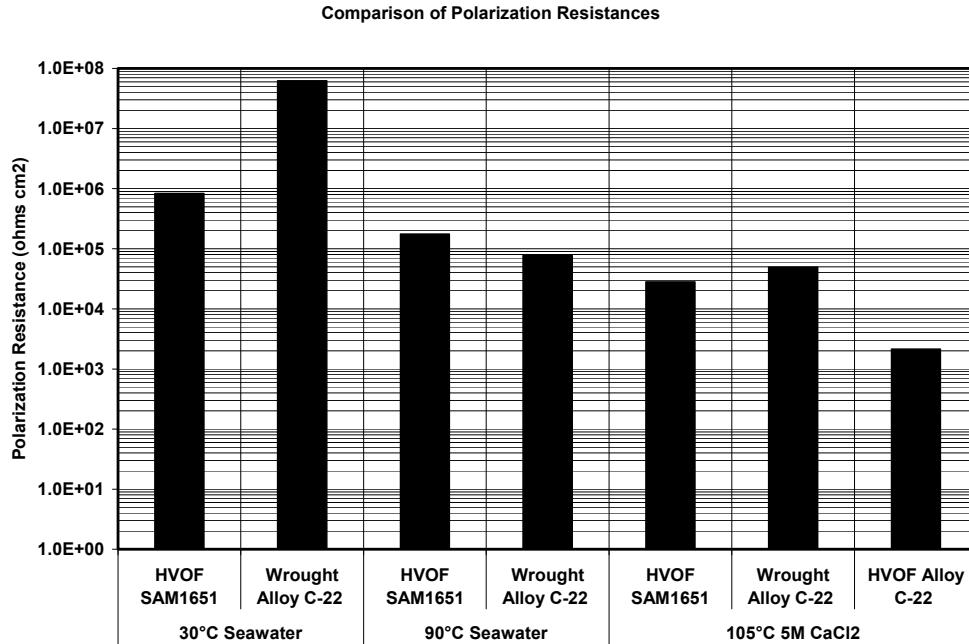**Comparison of Polarization Resistances**

Figure 15 – Linear polarization was used to determine the polarization resistance for thermal spray coatings of SAM1651 and the reference material (wrought nickel-based Alloy C-22) in three relevant environments, Half Moon Bay seawater at two temperature levels, and in hot concentrated calcium chloride (5M CaCl$_2$ at 105°C).

Comparison of Corrosion Rates Determined with Linear Polarization
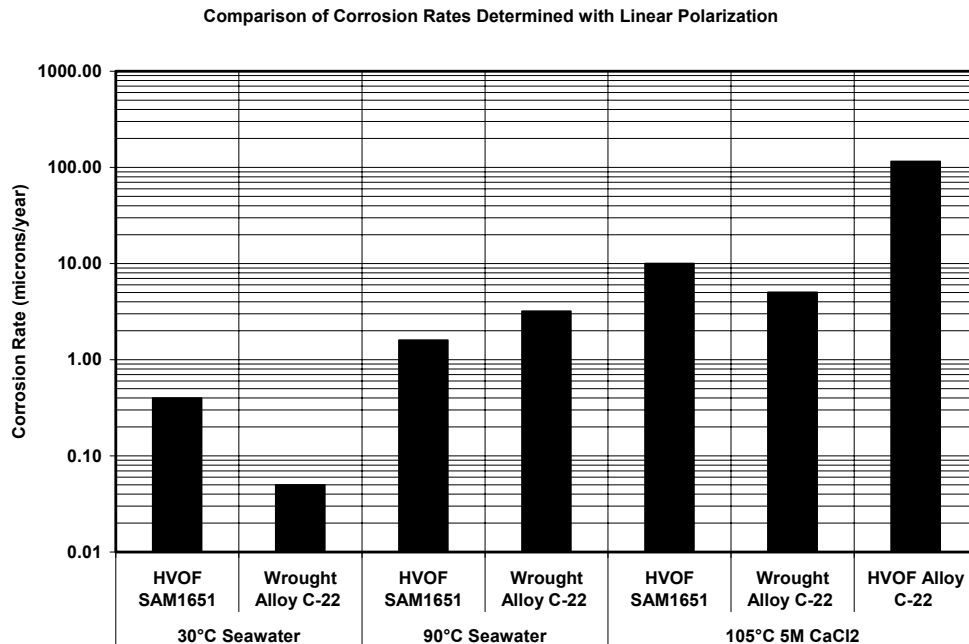

Figure 16 – Values of the polarization resistance shown in Figure 15 were converted to corrosion rates for the thermal spray coatings of SAM1651 and the reference material (wrought nickel-based Alloy C-22) in three relevant environments, natural seawater at two temperature levels, and in hot concentrated calcium chloride (5M CaCl$_2$ at 105°C).
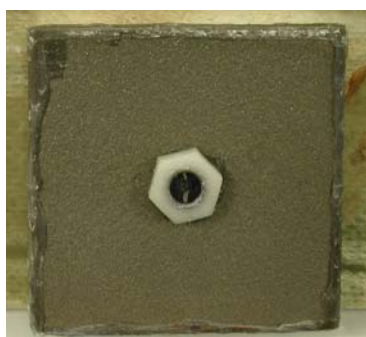
Type 316L Coating After Exposure for 13 Cycles

Original DAR40 After Exposure for 13 Cycles

SAM1651 (SAM7) After Exposure for 30 Cycles – No Corrosion at 60 Cycles

Figure 17 – Salt fog testing was conducted on several thermal spray coatings, including HVOF coatings of Alloy C-22, Type 316L stainless steel, SAM40 and SAM165. After 30 cycles in the standard GM salt-fog test, the HVOF coating of Alloy C-22 showed slight rusting (not shown), while the HVOF coatings of Type 316L stainless steel and SAM40 showed substantial corrosion. In contrast, the newer SAM1651 (SAM7) formulation showed no corrosion at 30 cycles. The salt fog testing ofSAM1651 (SAM7) was continued to almost 60 cycles with no evidence of corrosion.